Geochronology of monazite related to REE, Nb-Ta and U-Th bearing minerals from Mesoproterozoic anorogenic magmatism in the E-Colombian Amazonian Craton: links to mantle plume activity in the Columbia (Nuna) supercontinent

José Alejandro Franco Victoria, Thomas Cramer, Alexandre de Oliveira Chaves, Heinrich Adolf Horn, Marc Poujol

Geochronology of monazite related to REE, Nb-Ta and U-Th bearing minerals from Mesoproterozoic anorogenic magmatism in the E-Colombian Amazonian Craton: links to mantle plume activity in the Columbia (Nuna) supercontinent

Franco, José Alejandro[1,2]; Cramer, Thomas [1,2], Chaves, Alexandre de Oliveira[3]; Horn, Heinrich Adolf[2,3]; Poujol, Marc[2,4]

1. *Universidad Nacional de Colombia, Bogotá, Colombia. Corresponding author e-mail: jafrancov@unal.edu.co*
2. *Grupo de Estudios en Geología Económica y Mineralogía Aplicada (G.E.G.E.M.A)*
3. *Universidade Federal de Minas Gerais (UFMG), Av. Antonio Carlos 6627, 31.270-901 Belo Horizonte – Brazil*
4. *Univ Rennes, CNRS, Géosciences Rennes-UMR 6118, F-35000 Rennes, France.*

Abstract

U-Th-Pb geochronology of REE-bearing minerals such as monazite and other phosphates has become a precise tool to date mineralization events through geological time. In the E-Colombian Guainía department, from 3 colluvial sites over western Guiana Shield Mesoproterozoic rocks Nb-Ta, U-Th and REE bearing minerals probably of pegmatitic origin were sampled including up-to-0.5 cm long monazite crystals. The monazite pan concentrate samples from sites near to the indigenous communities of Barranquilla, San Jose and Chorro Bocón (Espina hills) along the Cuyari, Guainía, and Inírida rivers respectively, were analyzed geochemically and geochronologically using LA-ICP-MS and EPMA. The monazites obtained from the 3 sites are rather similar among each another and of approximate composition $Ce_{0.44}La_{0.16}Nd_{0.16}Sm_{004}Y_{0.03}Gd_{0.02}Dy_{0.01}Pr_{0.05}Th_{0.08}Pb_{0.01}Ca_{0.05}Si_{0.05}P_{0.91}O_{3.94}$. Their EPMA and LA-ICP-MS ages suggest at least two mineralization events, a first one between 1528 and 1523 Ma in the Barranquilla and San Jose sites, related to rapakivi granites outcropping along the Cuyarí River and the Tabaquen rapakivi granite near the Guainía River, both emplaced ~1545 Ma ago. The second mineralization event from 1390-1343 Ma recorded in the Espina-hills is in the age range of the Matraca and Danta rapakivi granites that crystalized between 1400 and 1340 Ma ago. These different anorogenic rapakivi granites were emplaced between 1550 and 1300 Ma into Mesoproterozoic basement rocks and were probably caused by intra-plate processes associated with mantle plume activity within the Columbia (Nuna) supercontinent.

Key words: monazite; U-Pb and EPMA geochronology; anorogenic magmatism; mantle plume; Columbia (Nuna) supercontinent.

1 Introduction

Due to their high ionic charge and large ionic radii, Rare Earth Elements (REE) are not easily incorporated within the early-crystallizing silicates (Winter, 2001). Instead, they are enriched in highly differentiated magmatic phases together with other incompatible elements (such as P, K, Rb, U, Th). Despite similar chemical properties, they may be partitioned by either geochemical, mineralogical, and petrological processes in which case they become valuable proxies to study them (Henderson, 1984).

Generally spoken, Light Rare Earth Elements (LREE) tend to be concentrated in pegmatites and carbonatites, whereas Heavy Rare Earth Elements (HREE) are concentrated in granitic magmas (Pirajno, 2009).

Monazite is a LREE phosphate with the generalized formula (LnIII, Th) (PO_4), where LnIII represents a trivalent light lanthanide, and is part of a complete solid solution with the LREE from La - Ce to Sm. Although present in most rock types, monazite is frequently found as an accessory mineral in low-Ca igneous rocks (Itano et al., 2016), instead of apatite and/or bastnäsite mineralization, and in differentiated magmatic phases like granites, syenites and granitic pegmatites. As monazite frequently occurs in colluvial and placer deposits, it is often better studied in these types of deposits than in the magmatic phases where they crystallized (Dill, 2010; Dill et al., 2012).

Elemental analyses of monazite can bring some information on its origin. For example, Itano et al. (2018) found that the La/Sm ratios in monazite grains from granite and granitic pegmatite and from magnetite and ilmenite magmas were different. This ratio could therefore be used as a good proxy for the type of magma. Although monazite can contain up to 12 wt% ThO_2 (Mottana et al., 1978) it is never metamict (Seydoux-Guillaume et al., 2018) and, such as zircon, usually does not incorporate initial lead when it crystallizes. Therefore, all the Pb comes from the radioactive decay of Th and U, which makes monazite a mineral suitable for U-Th-Pb dating via EPMA (electron probe micro analysis) (Itano et al., 2016) as described by Montel et al., (1996), Suzuki and Kato (2008) and Chaves et al., (2013). This type of analyses should however be used with caution as, in some cases, EPMA dating can fail to resolve different monazite age populations as demonstrated by Poujol et al. (2017). Their use as geochronometers by means of LA-ICP-MS (Laser ablation inductively coupled plasma mass spectrometry) and EPMA is compiled by Engi (2017) and Williams et al. (2017).

Crustal-melt rapakivi granites with their characteristic coarse zoned feldspar megacrysts in a finer matrix are probably the result of mantle plume activity (Pirajno, 2007). In eastern Colombia, several authors have reported ages between 1550 and 1340 Ma for anorogenic rapakivi granites such as the Parguaza, Danta, Matraca and Tabaquen intrusions (e.g. Bonilla et al., 2013, 2016; Cordani et al., 2016). In these granites, pegmatitic phases may host monazite, xenotime, columbite-tantalite, Nb-rich rutile as well as U oxides.

For this research, three localities in the E-Colombian Guainía Department were selected (Figures 1 and 2): Espina hills – near the Inírida river LOC (4), San José – near the Guainía river LOC (5) and Barranquilla – near the Cuyarí river LOC (6) where Mesoproterozoic pegmatite-related colluvial rock fragments contain centimetric Ti, Nb-Ta, U and Th bearing minerals together with monazite and xenotime. Here we present EPMA and LA-ICP-MS analyses performed on monazite crystals in order to determine their elemental compositions as well as their crystallization ages in order to understand their possible provenance within the western Guiana Shield, i.e. the NW-part of the Amazonian Craton.

Further we discuss pegmatitic phases with Ti, Nb-Ta, U-Th and REE mineralization in relation to the 1550-1340 Ma anorogenic granites found in various parts of the western Amazonian Craton in the light of intra-plate processes associated with mantle plume activity, which may have controlled this magmatism within the Columbia (Nuna) supercontinent.

2 Methods used

From panning concentrates (pc) more than 20 monazite crystals from each locality were picked and verified using a handheld Bruker Tracer III-V X-ray fluorescence instrument equipped with a Rh-tube and Silicon Drift Detector (SDD), working conditions 15-40kV, 5-10mA, 60-120s exposure time, no filter nor vacuum which together with the S1PXRF software allow to detect all elements heavier than Na (e.g. Magrini et al., 2018). Three epoxy resin pucks, labeled LOC (4), LOC (5) and LOC (6), each with ~10 crystals, were prepared using buehler epoxy cure2 resin and hardener, polished first with silicon carbide and diamond and then coated with graphite (Mange and Wright, 2007; Reed, 2005). Scanning electron microscopy (SEM) BSE images of the monazite crystals allowed choosing the most homogeneous zones, free of inclusions or in very low proportion. Their chemical composition was determined using wavelength-dispersive spectroscopy (WDS) in a JEOL JXA-8900 EPMA in the Laboratory of Microanalysis of the Microscopy Center at Federal University of Minas Gerais (LMA-CM-UFMG), Brazil. The reference materials used were Y_2O_3 (YAG_25K50n), Dy_2O_3 ($DyPO_4$_25K50n), P_2O_5 (Monaz_25K50n), SiO_2 ($ThSiO_4$_25K50n), Gd_2O_3 ($GdPO_4$_25K50n), PbO (Crocoi_25K50n), Sm_2O_3 (REE_2_25K50n), ThO_2 (ThSiO4_25K50n), Nd_2O_3 ($NdPO_4$_25K50n), UO_2 (UO_2_25K50n), Pr_2O_3 ($PrPO_4$_25K50n), CaO ($Ca_2P_2O_7$_25K50n), (Ce_2O_3) (Monaz_25K50n) and La_2O_3 (Monaz_25K50n). Additionally, 30 monazite crystals up-to-0,5 cm large from LOC (5) were analyzed. For EPMA dating, from each locality 1 monazite crystal from the polished epoxy pucks was selected, and ages were calculated using U, Th and Pb concentrations (Williams et al., 2007).

The EPMA-analyses were performed in 6 to 10 spots per crystal. Standards and quantitative WDS analytical parameters used during monazite analyses are described in Chaves et al. (2013). Overlaps of X-ray peaks between Y and Pb have not been corrected because there was no measurement in PbMa (Lead M

alpha), but only in PbMb (Lead M beta). However, to avoid errors in the obtained ages, the interference of ThMz (Thorium M gamma) on the measured UMb (Uranium M beta) had to be corrected, following Scherrer et al. (2000) in adaptation to the conditions of the LMA-CM-UFMG, as follows (Chaves et al. 2013):

U corrected = U measured – (0.006365 x Th measured).

Microprobe chemical U-Th-Pb_T ages and associated errors were obtained using EPMA Dating software (Pommier et al., 2004) and the average ages were taken through Isoplot/Ex software (Ludwig, 2003). The age equation used is:

$$Pb = \{Th \times [\exp(\lambda 232\mathrm{T}) - 1] \times (M208 / M232)\} + \{Uc \times [\exp(\lambda 238\mathrm{T}) - 1] \times (M206 / M238) \times 0.9928\} + \{Uc \times [\exp(\lambda 235T) - 1] - 1] \times (M207/M235) \times 0.0072\}$$

Where: $^{238}U/(^{235}U+^{238}U)$ = 0.9928 and $^{235}U/(^{235}U+^{238}U)$ = 0.0072. Uc (U corrected), Th and Pb are concentrations in ppm; T is the age in Ma; M206, M207, M208, M235, M238, M232 are the atomic masses of ^{206}Pb, ^{207}Pb, ^{208}Pb, ^{235}U, ^{238}U, ^{232}Th; $\lambda 232 = 0.49475 \times 10^{-4}$ Ma^{-1}; $\lambda 238 = 1.55125 \times 10^{-4}$ Ma^{-1}; $\lambda 235 = 9.8485 \times 10^{-4}$ Ma^{-1} (Pommier et al., 2004).

Ages and uncertainties were obtained using EPMA Dating software (Pommier et al., 2004) and age averages were processed using Isoplot 3.75 Excel version (Ludwig, 2012, 2003).

Beside the U and Pb values, also the other elements were used for unravelling both mineral chemistry and REE-geochemistry and calculate approximate mineral compositions assuming an idealized monazite formula $Ln^{3+}PO_4$ and considering all elements as part of the mineral lattice (i.e. not specifying possible inclusions or exsolutions of other phases). For the formulae calculations, mineralogical standard normalization procedures were applied (Deer et al., 2013; Perkins, 2014), i.e. the transformation of the mean oxide wt-% to mole-%, the distribution of the cations to the four anionic O-sites, and the calculation if the cation and anion charges became balanced.

LA-ICP-MS dating has been performed by using aleatory points in all crystals of the three sampling sites LOC (4, 5 and 6) including the same crystals analyzed by EPMA. Analyses were carried out on a single quadrupole Agilent 7700 ICP-MS mass spectrometer coupled to a 193-nm excimer laser system ESI (NWR193UC) in the GeOHeLiS analytical platform of the University of Rennes 1 in France. In the present study, the acquisition time of each analytical spot was set to 80 seconds (20 seconds background followed by 60 seconds with the laser firing). Spots diameters of 8 µm associated with repetition rates of 3 Hz with a laser fluency of 5 $J.cm^{-2}$ were used. The signal of $^{204}(Pb+Hg)$ ^{206}Pb, ^{207}Pb, ^{208}Pb, ^{232}Th and ^{238}U masses were acquired. The ^{235}U signal is calculated from ^{238}U based on the ratio $^{238}U/^{235}U$ = 137.818 (Hiess et al., 2012).

Data were corrected for U–Pb and Th–Pb fractionation and for the mass bias by standard bracketing with repeated measurements of the Moacir monazite reference material (Gasquet et al., 2010). Data reduction was carried out with the software package GLITTER® (Van Achterbergh et al., 2001). Repeated analyzes of the Manangoutry monazite reference material (Paquette and Tiepolo, 2007) treated as unknown were used to control the reproducibility and accuracy of the corrections and yield a concordia age of 548 ± 6 Ma (MSWD=0.98; n=11). After data reduction, U-Th-Pb Concordia diagrams were constructed with the IsoplotR software (Vermeesch, 2018). The calculated Concordia ages are quoted with 95% of confidence interval. More information on the analytical protocol in Poujol M, et al., (2017) and supplementary table in Annex. A.

3 Geological background

The Guainía Department is located at the northwestern part of the Guiana Shield i.e. a portion of the Colombian part of the Amazon Craton, which extends from the Andean Eastern Cordillera foothills to Venezuela and Brazil and is the least populated and studied area of Colombia. Our geological knowledge of this area is largely based on research conducted in Brazil and Venezuela (e.g., Gansser, 1954, 1974; Amaral, 1974; Gaudette et al., 1978; Almeida et al., 1981; Gaudette and Olszewski, 1985; Bettencourt et al., 1999; Tassinari et al., 1999 and (Santos et al., 2000), although important studies have been done recently also in Colombia (e.g., Bonilla et al., 2013, 2016, 2019; Cordani et al., 2016, Ibanez et al., 2011, Kroonenberg, 2019).

According to Santos (2003), the crystalline basement in the Western Guiana Shield is linked to the Rio Negro geochronological province 1.82 – 1.52 Ga (Figure 1).

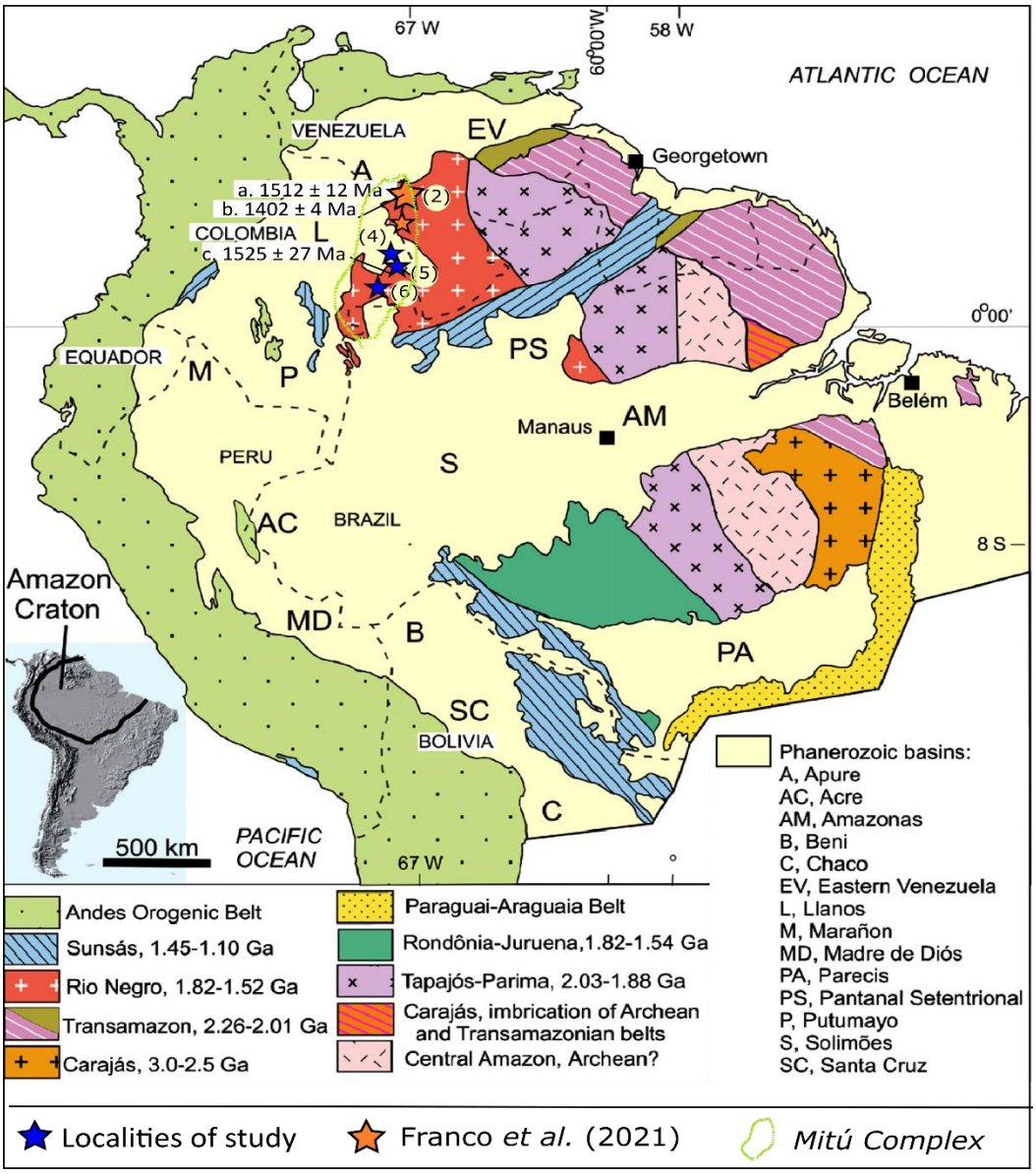

Figure 1. Regional map showing the geochronological provinces and some ages in Ma reported for rocks and minerals in and outside the study area: a. U-Pb in rutile (Nb,Ta) from Cachicamo hills; b. U-Pb in zircon from the basement zone (Bonilla et al., 2013); c. U/Pb in zircon from granitic rocks of Tabaquen in the Guainía River Bonilla (2019). Modified from Santos et al. (2008).

Enhanced by the PRORADAM program (Galvis Vergara et al., 1979a; Huguett et al., 1979) the complex geological history of Colombia since the Proterozoic has been slowly revealed, with different phases of extension and compression, orogenesis, erosion, sedimentation, metamorphism and emplacement of a wide variety of magmatic rocks. Hallmarks in descriptions represent Celada et al. (2006) and recently Kroonenberg (2019) synthetized the actual geological information of E-Colombia.

Different orogenic episodes in the Guiana Shield have been recognized so far (Kroonenberg 2019): the Transamazonian Orogeny (2.26 to 1.98 Ga) in the Eastern margin (as result of the collision with Proto-Africa); the Querarí Orogeny (1.86–1.72 Ga) at the Western border between Colombia, W-Venezuela and NW-Brazil; and, in the framework of the Rodinia supercontinent formation, the Grenvillian Orogeny (1.3–1.0 Ga), called Putumayo Orogeny by Ibáñez-Mejía et al. (2011) as revealed by some inliers in the Andes but also eastward by gabbroic intrusions (Bonilla Perez et al., 2020).

In the Guainía Department between the Guaviare River to the north, the Caquetá River to the south, and the Chiribiquete mountain range to the west only very few outcrops have been studied in the past. The oldest rocks seem to be felsic to intermediate metavolcanic rocks along the Atabapo River and parts of the Río Negro River, which Galvis et al. (1979) and Huguett et al. (1979) named “Neises del Atabapo-Río Negro” (see López et al., 2010). Kroonenberg (2019) proposed that they do not belong to the Mitú-Complex but rather to the Mid-Paleoproterozoic Caicara Metavolcanics and associated them with the 1984 ± 9 Ma Surumu Rhyodacite (SHRIMP U-Pb in zircons, Santos et al., 2003).

The Colombian basement was first described as the “Basement Group” (Gansser, 1954) or as the “Guyanese Complex” (Pinheiro et al., 1976), then as the Migmatitic Mitú Complex (Galvis Vergara et al., 1979b) and later as the Mitú Complex (López Isaza, 2012; López Isaza et al., 2007; López Isaza and Cramer, 2012). Its extension has been initially inferred based on geophysical data. Most of this basement is constituted by Precambrian crystalline rocks. It is covered by Cenozoic sediments, as well as by a thick tropical forest covering peneplanes modeled by strong tropical weathering and meandering rivers in extensive alluvial plains, locally interrupted by inselbergs of the old basement.

The Mitú Complex is composed of high-grade metamorphic rocks and granitoids with various compositions and affinities, formed during different orogenic events (Kroonenberg, 2019; López Isaza et al., 2007). The metamorphosed igneous and sedimentary protoliths appear mainly as quartz feldspathic gneisses with alaskite to monzonite composition, but also as amphibolite, quartzite, metagranitoids, calco-silicate (rich in epidote group minerals) and quartz gneisses, some of them with migmatitic structures.

Large parts of the Mitú Complex (Figure 2) are composed of monzogranites with calc-alkaline affinities, besides meta- to peraluminous granites (U-Pb in zircon LA-MC-ICP-MS Concordia age of 1574 ± 10 Ma for the Mitú granite; Ibáñez-Mejía et al., 2011), as well as of other granites. Among the clearly metamorphic rocks, quartz-feldspathic gneisses are the most abundant with U-Pb zircon ages between 1800-1760 Ma (Bonilla et al., 2019; Cordani et al., 2016; Kroonenberg, 2019; López et al., 2007). Medium grade amphibolite facies metamorphic rocks within a series of essentially juvenile magmatic arcs in the Rio Negro Juruena province are interpreted by several workers as subduction-related (Cordani et al., 2016; Tassinari and Macambira, 1999).

Younger granitoids in the southeastern part (especially Guainía Department) exhibit variable compositions, porphyritic textures and may contain feldspar phenocrysts. They were emplaced ca. 1750 Ma ago during the Statherian (Bonilla et al., 2019) while some two-mica granite intrusions are 1600-1550 Ma old (Bonilla et al., 2019). It must be noticed that other ~1600 – 1500 Ma old granites have been described along the whole Colombian eastern territory (Cordani et al., 2016; Ibañez, 2010; Priem et al., 1982; Rodriguez et al., 2011).

The Parguaza batholith, emplaced 1550-1500 Ma ago, represents a primary source of Sn, Nb, Ta and REE mineralization (Aarden and Davidson, 1977; Herrera-Bangerter, 1989; Mariño, 2012; 2013) although it is largely covered by partially lateritic Cenozoic sediments in plains and valleys. In the Venezuelan localities of El Burro, La Fortuna and Aguamena, colluvial - alluvial deposits contain sub-to economic concentrations of minerals such as cassiterite, rutile-(Nb,Ta), columbite-tantalite and REE minerals.

An important feeder of rare element minerals in the Parguaza Batholith seem to be pegmatites, and similarly pegmatites associated to the Mitú Complex (e.g. López Isaza and Cramer, 2012) may also be the main primary source of the monazites and xenotimes discussed here.

4 Pegmatites

Due to their economic importance and variability, manifold pegmatite classification efforts (e.g. Ginsburg et al., 1979) were developed over time which are still controversial and object of research. Thus Černý (1991) proposed the existence of two main pegmatite families, the LCT (Li-Cs-Ta) and the NYF (Nb-Y-F), a concept however only applicable for highly fractionated pegmatites if exotic minerals such as spodumene, tantalite, pyrochlore, pollucite, etc. are present (London, 2018). Černý and Ercit (2005) and Černý et al. (2012) defined, based on metamorphic environment, mineralogy, elemental composition and texture, five pegmatite classes from which four may host Ta–Nb–Sn mineralization (especially the abyssal, muscovite-rare-element, rare-element and miarolitic classes) and 10 subclasses. The rare-element class is the most important for Nb–Ta mineralization, which are further subdivided depending on major and minor minerals carrying Li, Be, REE and Nb–Ta.

Most of the pegmatites with the LCT signature have compositional affinity with S-type granites (Chappell and White, 1974, 2001). Their protoliths are assumed to be pelitic marine sediments as source of Al - and trace elements enrichment like B, Be, P and Sn. From those after anatectic melting of metamorphic schists and gneisses, reduced granites and derived specialized pegmatites could form with high contents in Li, Cs, Ta where fluxing components like B, P, and F play an important role. Many of these trace elements with different grades of incompatibility are contained in micas and feldspars and liberated during the melt-forming reactions and may concentrate furthermore in specialized pegmatites above the mineralization limit, i.e. forming abundant and large visible minerals

characteristic of many famous and economic important pegmatite ore deposits worldwide.

On the other hand, most of the NYF-family pegmatites are thought to be derived from A-type granites, where “A” may mean “anorogenic” (e.g. Eby, 1990) but also Al-rich or abnormal and their origins are debatable. For example, Frost and Frost (2014) emphasized their higher Fe-content and proposed to name them ferroan alkali-calcic to calc-alkalic granitic rocks. Their source may be gneissic granulites deep in the continental crust, with some mafic mantle contribution or low-density carbonic fluid. The NYF-family contains chemically complex oxides and silicates that carry heavy rare earth elements (HREE), Ti, U, Th, and Nb > Ta (Cerný et al., 2012). Abundant fluorite or topaz reflects the enrichment in fluorine. The NYF pegmatites are depleted in phosphorus, and tourmaline is uncommon.

Subduction-related I-type granites may be a smaller source both of LCT and NYF pegmatites (Černý and Ercit, 2005), but there are a lot of pegmatites worldwide, which may or may not fit clearly in any of these models (Bonin, 2007; Cerný et al., 2012; Dall’Agnol et al., 1999; Dill, 2015; Dill et al., 2006; Gandhi and Sarkar, 2016; Kroonenberg et al., 2016; Laznicka, 2006; London and Morgan, 2012; Sial et al., 2011).

5 Selected mineral occurrences

The Guainía region is mostly covered by humid tropical forests and extensive alluvial plains with preferably west-east drainage of the main rivers Guaviare, Inírida, Guainía and Cuyarí to the Orinoco and Amazonas rivers, which constitute also the main ways of communication between local indigenous communities and non-local population. During several fieldtrips, sediments and basement rocks outcropping along the main rivers including inselbergs like Mavicure, Espina, Tortuga, Tabaquen, Matraca and Danta were sampled, and from Vichada to Guainía departments, four localities from north to south were defined for more detailed studies and are described elsewhere, especially the Cachicamo rutiles-(Nb), closely associated to the Parguaza Batholith (Franco et al., 2021). For this study, we analyzed three of them in the Guainía Department (Figure 2): LOC (4) near to the Inírida River and the Espina hills, LOC (5) near to San Jose at the Guainía River, and LOC (6) near to Barranquilla at the Cuyari River.

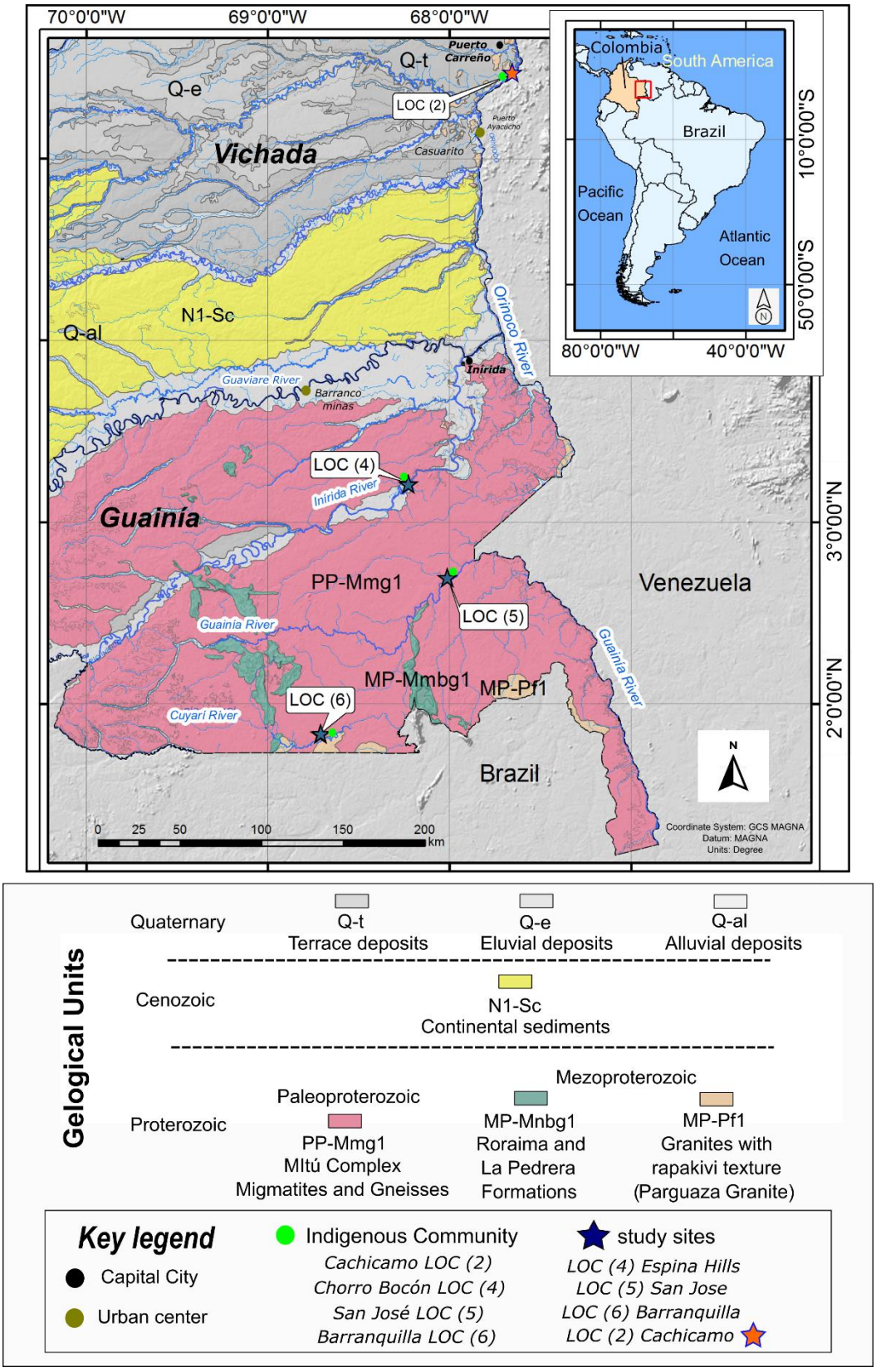

Figure 2. Generalized geological map of Vichada and Guainía Department, eastern part of Colombia showing the localities (4, 5 and 6) (blue stars) and locality (2) (pink star) -

from which localities (4 to 6) were selected for this study; locality (2) associated to the Parguaza Granite was studied by Franco et al., (2021) and is here shown for a better overview. As green dots the names of the communities nearby the sampling locations. Modified from the Geological Map of Colombia (Gómez Tapias et al., 2015).

5.1 Monazite, xenotime and Nb, Ta, U, Zr-minerals from Espina hills - Inírida River LOC (4)

In the Espina foothills as main mineralization site of LOC (4) N 03° 12' 13.6'', W 068° 09' 19.6'' (Figure 2), monazite occurs in colluvial deposits with large blocks of quartz and muscovite pegmatites. Monazite crystals can reach up to 1 cm in length and are associated with rutile-(Nb,Ta), xenotime, REE-enriched zircon and U-Th bearing minerals and, in some cases, black tourmalines in the panning concentrates (Figure 3).

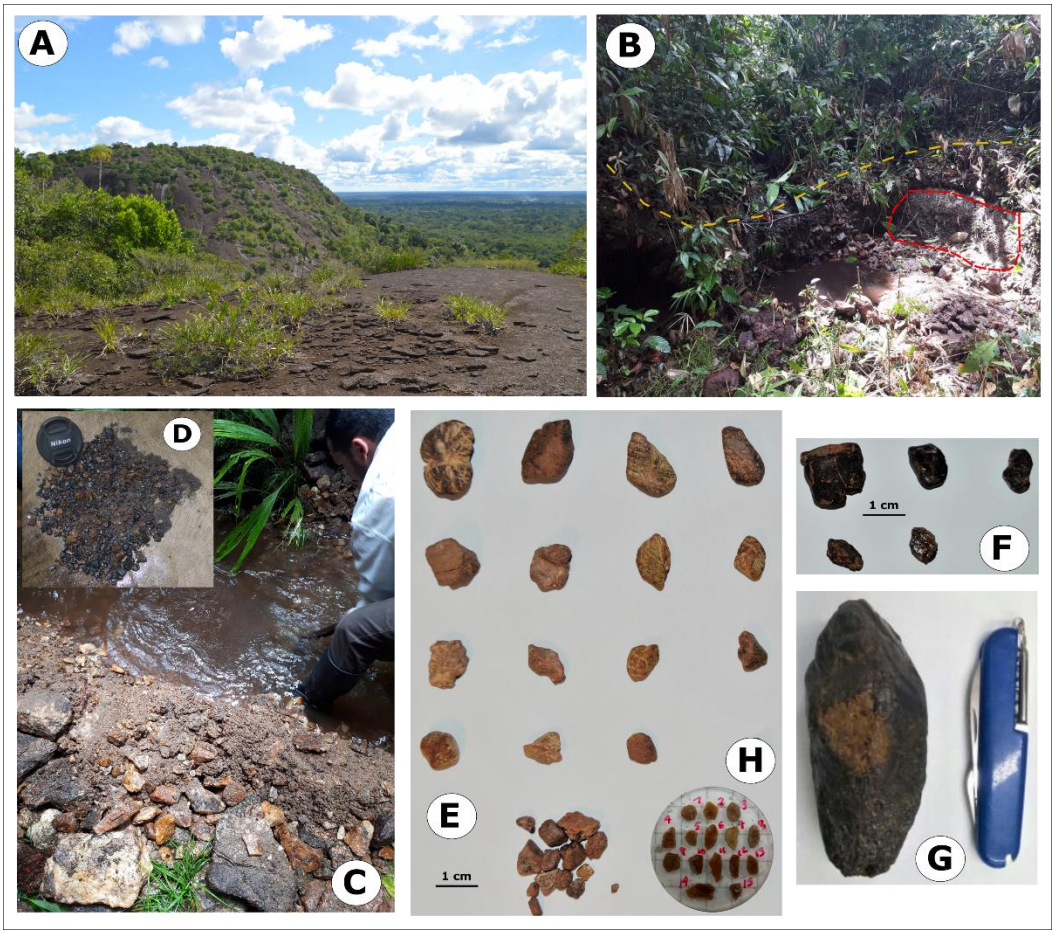

Figure 3. Pictures of field and mineral found in panning concentrates from LOC (4) Espina Hills. A. view from the top of Espina Hills; B. colluvial deposits in the foothill of Espina Hills (yellow line shows the limit of the dissectect colluvium and red line basement rock); C and D. sample site and heavy mineral concentrate and pan concentrate, respectively; E. Monazite and xenotime crystals selected from the pan concentrates; F. U-Th bearing minerals; G. Rutile-(Nb) associated to monazite (brown color) and H. Polished epoxy resin puck of monazite for analysis.

5.2 Monazite and Ta, Nb-minerals at the San Jose - Guainía River LOC (5)

Near to the Indigenous community of San José labelled LOC (5) N 02° 41’ 59.6’’, W 068° 01’ 38.4’’ (Figure 2), monazite grains were found in the regoliths overlying pegmatitic dykes emplaced in gneiss and migmatites of the Mitú Complex. However, the most representative crystals occur in colluvium deposits together within blocks and gravels of quartz and muscovite dyke fragments along the Seje and Lombriz creeks. Monazite crystal can reach up to 3 cm in length and are found together with Fe-columbite, rutile-(Nb,Ta) and magnetite (Figure 4). Occasionally isolated xenotime and tourmaline crystals are found in the panning concentrates.

Figure 4. Pictures of field and mineral found in panning concentrates from LOC (5) San Jose. A. view of rocks of Mitú complex in the Guainía River at San Jose indigenous community; B. Pegmatite with an elevated radioactivity measures; C. Pegmatite with Fe-columbite crystal; D. Sample site of heavy mineral concentration E. Fe-columbite crystals from pan concentrates; F; Huge monazite crystals from pan concentrates; G. Monazite crystals selected from the pan concentrates and H. Polished epoxy resin puck of monazite for analysis.

5.3 Monazite and Ta, Nb, Zr and REE-minerals from Barranquilla - Cuyari River LOC (6)

Monazite grains were found near Barranquilla labelled LOC (6) N 01° 48’ 51.9’’, W 068° 41’ 12.5’’ (Figure 2), in colluvium deposits cut by small drains along the

Cuyari River basin, together with smoky quartz blocks, muscovite, beryl and Fe-columbite dikes as well as K-feldspar, quartz and garnet bearing dikes. They are related to plutonic rocks from syeno-granites to acidic granites, some of them with rapakivi texture. Monazite can reach up to 0,5 cm in length and are found together with Fe-columbite, Mn-Tantalite, rutile-(Nb,Ta), xenotime, zircon, and garnet (spessartine) (Figure 5). Isolated crystals of black tourmaline occasionally occur in panning concentrates.

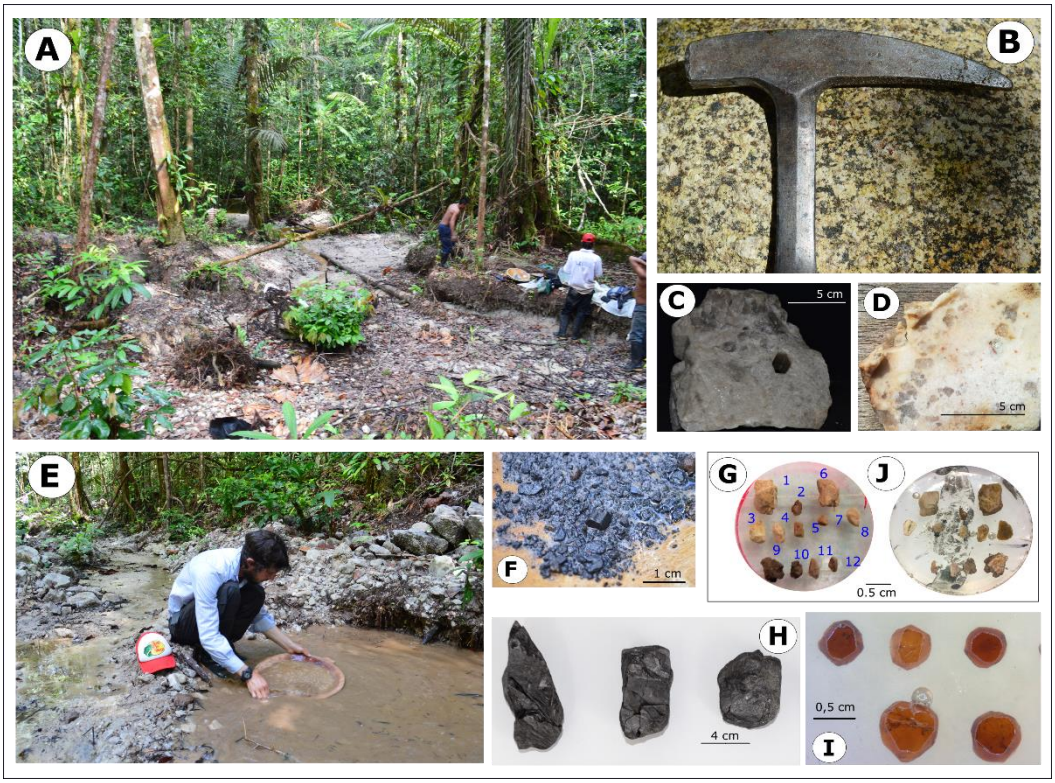

Figure 5. Pictures of field and mineral found in panning concentrates from LOC (6) Barranquilla. A. Colluvial deposits explored by local people from Barranquilla indigenous community; B. Block of two mica granite founded in the base of colluviums; C. Pegmatite with a retaining the shape of a beryl crystal y D Sample of K-feldspar - garnet pegmatite; E. Sample site of heavy mineral; F. Heavy mineral concentrate; G. Monazite crystals selected from the pan concentrates (1-5); H. Columbite-tantalite crystals; I. Garnet crystals and J. Polished epoxy resin puck of monazite for analysis.

6 Results

6.1 Monazite chemistry

The pXFR-measurements were in good qualitative agreement with the EPMA data (supplementary Table in Annex A) which reveal that all the monazite crystals are Ce and La dominated. As the BSE-images Figure 7 show very inclusion-poor monazites, the calculated mineral formulae should be very near to the real monazite compositions. The HREE Ho, Er, Tm, Yb and Lu were below EPMA-detection limit. In LOC (4), monazite grains are very homogeneous with Ce_2O_3 between 29 and 31% and ThO_2 between 8 and 9 %. The standard deviation

among the 7 measured monazite crystals of the main cations is below 0,1%. Their average formula including all elements could be expressed as $Ce_{0.44}La_{0.16}Nd_{0.16}Sm_{0.04}Y_{0.03}Gd_{0.02}Dy_{0.01}Pr_{0.05}Th_{0.08}Pb_{0.01}Ca_{0.05}Si_{0.05}P_{0.91}O_{3.94.}$

Monazite crystals from LOC (5) show a more heterogeneous composition with Ce_2O_3 between 27 and 34% and ThO_2 between 4 and 13 % resulting in standard deviations (n=8) of 7% for Th, and around 1% for La, Ce, Sm and Ca.

Their average formula would be $Ce_{0.44}La_{0.16}Nd_{0.14}Pr_{0.04}Sm_{0.04}Y_{0.03}Gd_{0.02}$ $Dy_{0.01}Th_{0.09}Ca_{0.07}Pb_{0.01}Si_{0.05}P_{,0.91}O_{3.94}$.

In LOC (6), monazite grains are still less heterogeneous than in LOC (4) and LOC 5 with Ce_2O_3 between 26 and 29% and ThO_2 between 9 and 12 %. The REE standard deviations (n=10) are around or below 0,1%. Their average formula would be:

$Ce_{0.42}La_{0.13}Nd_{0.19}Pr_{0.05}Sm_{0.05}Y_{0.05}Gd_{0.02}Dy_{0.01}Th_{0.10}Ca_{0.04}Pb_{0.01}Si_{0.08}P_{0.86}O_{3,94}$.

In all 3 sites, the sum of cations including P is 2, assuming an idealized monazite formula $LnPO_4$. Phosphor and oxygen deficits in all the formulas of the three sites are probably due to cation charge balance vacancies, especially of $Ce(^{3+}, ^{4+})$, and possible occupancy of elements like Si on the P-site.

Also, the chondrite-normalized REE distribution patterns in Figure 6 for the monazite crystals from LOC (4, 5 and 6) are very similar among each another. Their REE pattern is much closer to granitic than pegmatitic monazites as defined by Zhu and O´Nions (1999), especially exhibiting higher La and Ce contents than the pegmatitic reference monazites. The Gd and Dy depletion is characteristic of the monazite structure, and HREE enter preferentially in minerals like xenotime, as garnet is nearly absent.

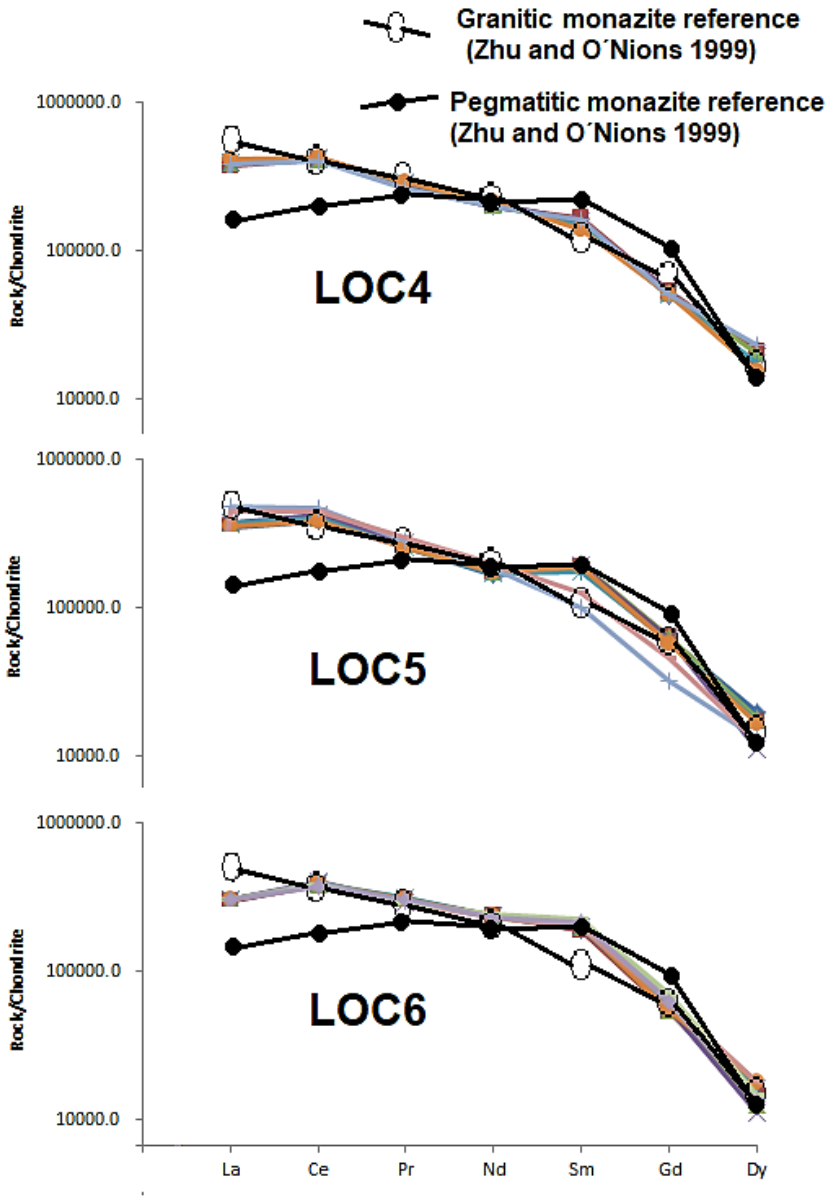

Figure 6 Chondrite-normalized (Sun and McDonough, 1989) REE patterns of the investigated monazites (Ho, Er, Tm, Yb and Lu below EPMA-detection limit) and comparison with pegmatitic and granitic monazites after Zhu and O´Nions (1999). Observe the higher coincidence of E-Colombian monazites with those of granitc origin with higher La and Ce in comparision to Zhu and O´Nions (1999) pegmatitic monazites.

6.2 Geochronology

6.2.1 EPMA U-Th-Pb chemical ages

Th and Pb contents of all dated monazite grains are relatively high which helps to minimize background related errors (Jercinovic et al., 2008). Seven analyses of the monazite crystal from LOC (4) in Espina Hills yield an EPMA age of 1390 ± 17 Ma (2σ, MSWD = 0.59) (Figure 7A). Eight analyses from the San Jose monazite crystal LOC (5) return a chemical age of 1523 ± 20 Ma (2σ, MSWD = 1.3) (Figure 7B). Ten spots on a single monazite grain from Barranquilla LOC (6) yield a chemical age of 1527 ± 13 Ma (2σ, MSWD = 0.27) (Figure 7C).

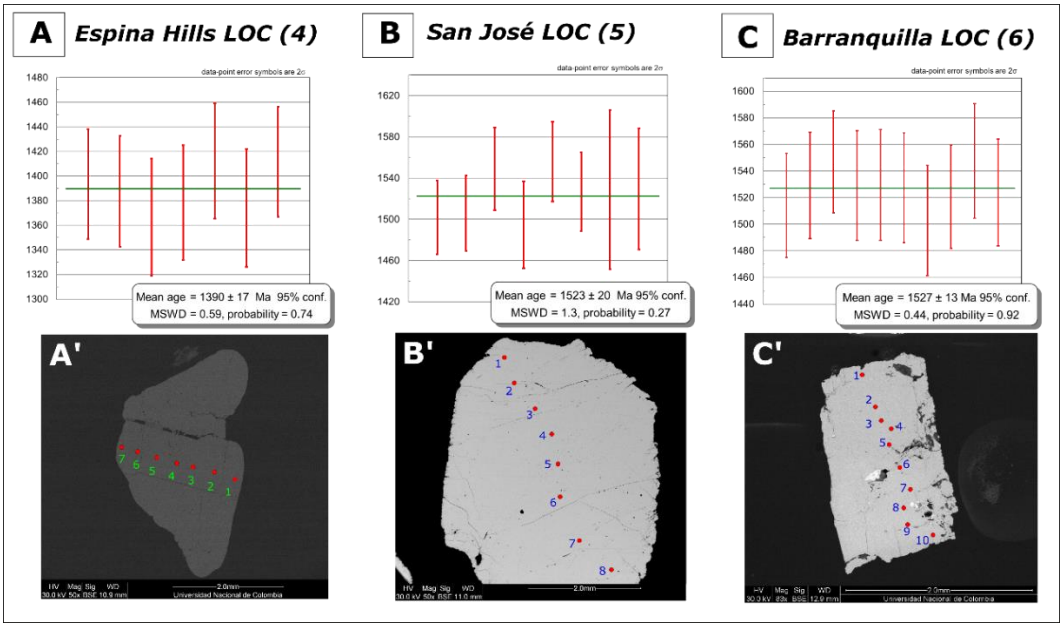

Figure 7. EPMA U-Th-Pb average ages calculated for each sample corresponding to Espina Hills (A), San José (B) and Barranquilla (C) localities. Data point errors are reported as 2σ. Below, BSE images of the corresponding monazite crystals showing the analyzed points (A', B' and C'). Data table in Annex B.

6.2.2 LA-ICP-MS U-Th-Pb ages

The twenty-two analyses in 15 monazite grains from LOC (4) expressed as $^{208}Pb/^{232}Th$ versus $^{206}Pb/^{238}U$ concordia diagram (Figure 8A) plot all in a concordant position and yield a concordia age of 1346 ± 18 Ma (MSWD (conc+equiv) = 1).

The fourteen analyses in 10 monazite grains of sample LOC (5) plot all in a concordant position (Figure 8B). Although they spread along the concordia curve with apparent ages from 1606 down to 1468 Ma, they yield a relatively well constrained concordia age of 1525 ± 15 Ma (MSWD (conc+equiv) = 1.9).

The fourteen analyses in 5 monazite grains of sample LOC (6) plot in a concordant position (Figure 8C). Two analyses (grey lines in Figure 8C) yield apparent ages of 1605 and 1650 Ma, respectively. However, the twelve remaining analyses yield a well-constrained concordia age of 1522 ± 16 Ma (MSWD (conc+equiv) = 1).

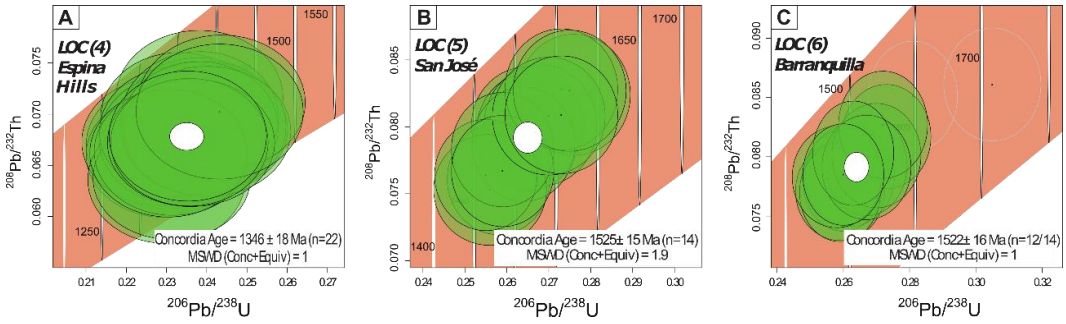

Figure 8. LA-ICP-MS monazite concordia ages of localities 4-6: Espina Hills (A), San José (B) and Barranquilla (C). Data table in Annex C. Data errors are reported at 2σ.

7 Discussion

7.1 Chemical data

The samples from this study were collected at the surface from colluvial deposits, weathered zones, and rock fragments, without the possibility of studying the magmatic to pegmatitic bodies present at depth. However, the geological, mineralogical, and geochemical data allow us to draw some preliminary, although contradictory conclusions about the three sites.

The chemical data suggest that the monazite crystals from all sites are very similar despite their distance of 70-150 km among each another. They are consistent with a granitic to pegmatitic origin, but without reaching highly specialized rare elements pegmatite characteristics. Parts of the mineral assemblage are indicative of a NYF-family affinity, with a geochemical signature Nb>Ta, Ti, Y, Sc, REE, Zr, U, Th, F (Černý and Ercit, 2005).

Melcher et al. (2017) proposed a possible NYF-family affinity for placer tapiolite, ixiolite, CGM (columbite group minerals) and rutile samples from not specified E-Colombian sites. One of their columbite, rutile and ixiolite samples however was collected near Barranco Minas at the Guaviare River (Figure 2). The presence of cassiterites and some personal information from the authors demonstrate that most of these samples were collected within the Vichada Department associated with the Parguaza Rapakivi Granite intrusion (see LOC (2) in Figure 2), which is also in agreement with the higher Sn-contents reported by Melcher et al., (2017). However, cassiterites were not found in panning concentrates in the Guainía Department study area. In the ixiolite and CGM-samples those authors also observed a CI-chondrite normalized HREE-enrichment trend and negative Eu and Y anomalies (Melcher et al., (2017).

Chappell and White (2001) recognized based on whole rock geochemistry an elevated phosphorus content as diagnostic of the S-type granites, and hence of LCT-pegmatites, whereas the NYF pegmatites are depleted in phosphorus,

tourmaline is uncommon and abundant fluorite or topaz would reflect the enrichment in fluorine (Cerný et al., 2012). If this is true, the abundant monazite, xenotime, and black tourmaline concentrations in the three sampling sites as well as the absence of fluor-bearing minerals advocate against a NYF affinity. The REE-monazite data of Zhu and O´Nions (1999) suggest a more granitic than pegmatitic origin of the mineralizations but are only one indication. Also, as the samples are from colluvial deposits, it may be that the two families of pegmatites (LCT and NYF) have been eroded and contributed to the overall chemical and mineralogical composition of the studied samples. We can therefore at this stage conclude that the mineralogical and geochemical data are not very conclusive to propose a clear affinity but support a more complex genesis that involve different primary sources related with S- and A-type granites from which mineralized pegmatites may have evolved.

7.2 Age and interpretations

We used EPMA and LA-ICP-MS as complementary technique, EPMA in this study was use for acquiring the chemical composition of the monazite as well as for calculating the chemical age while LA-ICP-MS was used to measure the isotopes U-Th-Pb for calculating directly the ages in a faster way which is better to do provenance analysis. LOC (5 and 6) yield an EPMA chemical and LA-ICP-MS ages of 1523 ± 20 Ma and 1525 ± 15 Ma and 1527 ± 13 Ma and 1522 ± 16 Ma respectively, all within the error, however LOC (4) yield an EPMA chemical and LA-ICP-MS ages of 1390 ± 17 Ma and 1346 ± 18 Ma respectively, a difference of ~45 Ma was found. This difference may be attributed to EPMA measurements due to imperfections in polishing. BSE Images (Figure 9) revealed a homogeneous non-zoned without inclusion monazite crystals for the three localities. For the other hand xenotime from the same pan concentrate used for LOC (4) yield an LA-ICP-MS U-Pb age of 1390 ± 8 Ma (unpublished data yet) that coud be related.

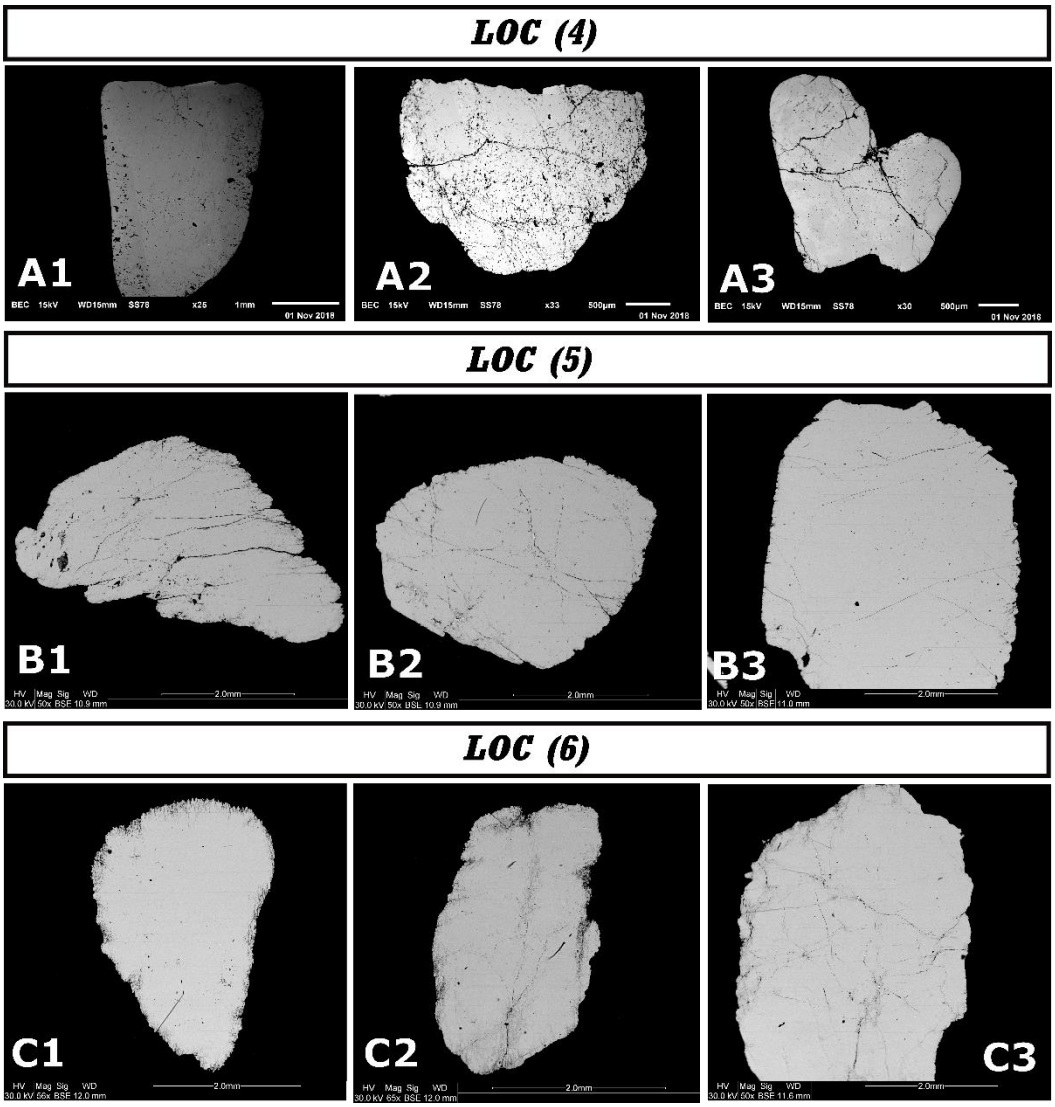

Figure 9. BSE images for some crystals use for LA-ICP-MS dating for the three localities showing a very homogeneous crystals of monazite. showing a rich thorium mineral were observed; (A1, 2 and 3) Monazite crystals from LOC (4); (B1, 2 and 3) Monazite crystals from LOC (5), small inclusion < 30 µm of Th mineral was observed; (C1, 2 and 3) Monazite crystals from LOC (6).

7.2.1 Age relation with the surrounding rocks

The oldest EPMA and LA-ICP-MS based ages at LOC (4) 1390 ± 17 Ma and 1346 ± 18 Ma, LOC (5) 1523 ± 20 Ma and 1525 ± 15 and LOC (6) 1523 ± 20 Ma and 1525 ± 15 Ma, respectively, indicate a crystallization age similar to Mesoproterozoic anorogenic intrusions recorded in homogeneous anorogenic A-type granites present in the study area (Table 1). This magmatic episodes represented by anorogenic granites in the surroundings of the Orinoco, Guainía, Inírida and Cuyari Rivers may be locally related with coeval granites from Vaupés River and regionally with rapakivi granites of the Pijiguaos range and Parguaza in

Venezuela with reported ages of 1545-1500 Ma and in Brazil with granites from the intrusive suite of Serra da Provincia with U-Pb ages of 1600-1532 Ma (see Table 1), intruded at the end of the Rio Negro Juruena orogeny. Several of these intrusive rocks and their post magmatic phases are the primary source of Sn, Ta, Nb and Ti mineralizations.

The crystallization ages obtained from the monazite crystals from the three localities are comparable with those from exposed Mesoproterozoic rocks such as Parguaza in Venezuela and Vichada, Colombia from Orinoco River, Danta and Matraca granites from the Inírida River, Tabaquen and similar granites from the Guainía River and the rapakivi granites from the Cuyarí River reported in the Guainía Department (see Figure 2 and Table 1)). The oldest obtained age range of 1527-1525 Ma from the localities (5, 6) may correspond to monazite mineralization from pegmatitic rocks related to granites near to Tabaquen and San José with U-Pb ages of 1606-1525 Ma and rapakivi granites at Cuyarí River with ages between 1550 -1600 Ma, and the younger ones in the locality (4) with an age range of 1346 to 1390 Ma could correspond to monazite mineralization from pegmatites of Espina, Danta and Matraca granitic rocks, the last one with an age of ~1343 Ma (Table 1).

Table 1. Compiled ages of some Mesoproterozoic granites from Colombia, Venezuela, and Brazil including the isotopic method use to dating

Locality	Country	Isotopic system	Age (Ma)	Reference
Murciélago Hill (Rapakivi granite)	Colombia	Ar/Ar	1237 ± 13	SGC (2013)
Murciélago Hill (Rapakivi granite)	Colombia	Ar/Ar	1292 ± 8	SGC (2013)
Angelita Hill (Rapakivi granite)	Colombia	Ar/Ar	1359 ± 8	SGC (2013)
Bita Hill (Rapakivi granite)	Colombia	Ar/Ar	1361 ± 9	SGC (2013)
La Hormiga Hill (Rapakivi granite)	Colombia	Ar/Ar	1359 ± 8	SGC (2013)
La Hormiga Hill (Rapakivi granite)	Colombia	Ar/Ar	1339 ± 8	SGC (2013)
La Hormiga Hill (Rapakivi granite)	Colombia	Ar/Ar	1366 ± 9	SGC (2013)
La Hormiga Hill (Rapakivi granite)	Colombia	Ar/Ar	1366 ± 9	SGC (2013)
La Hormiga Hill (Rapakivi granite)	Colombia	Ar/Ar	1376 ± 14	SGC (2013)
La Hormiga Hill (Rapakivi granite)	Colombia	Ar/Ar	1383 ± 8	SGC (2013)
La Venturosa (Rapakivi granite)	Colombia	Ar/Ar	1368 ± 14	SGC (2013)
La Venturosa (Rapakivi granite)	Colombia	Ar/Ar	1361 ± 8	SGC (2013)
Tomo River (Rapakivi granite)	Colombia	U/Pb	1392 ± 5	Bonilla et al. (2013)
Cachicamo Hills (Rapakivi granite)	Colombia	U/Pb	1402 ± 2	Bonilla et al. (2013)
Inírida River, Matraca and Danta rapakivi granites	Colombia	U/Pb	1343 ± 8	Bonilla et al. (2016)

Locality	Country	Isotopic system	Age (Ma)	Reference
Apaporis River (Syenogranite)	Colombia	U/Pb	1593 ± 06	Ibañez-Mejia et al. (2011)
Apaporis River (Syenogranite)	Colombia	U/Pb	1578 ± 27	Ibañez-Mejia et al. (2011)
Apaporis River (Monzogranite)	Colombia	U/Pb	1530 ± 21	Ibañez-Mejia et al. (2011)
Vaupés River (monzogranite)	Colombia	U/Pb	1574 ± 10	Ibañez-Mejia et al. (2011)
Mitú granite	Colombia	U/Pb	1552 ± 34	Priem et al. (1982)
Raudal Morroco Inírida River (Monzogranite)	Colombia	U/Pb	1507 ± 22	Cordani et al. (2016)
Mitú range (Monzogranite)	Colombia	U/Pb	1510 ± 26	Cordani et al. (2016)
Matraca granite - Inírida River	Colombia	U/Pb	1343 ± 8	Bonilla et al. (2016)
Granites of the Guainía River	Colombia	U/Pb	1606 ± 46	Bonilla et al. (2019)
Granites of the Guainía River	Colombia	U/Pb	1525 ± 27	Bonilla et al. (2019)
Cuyari River (Porphyritic granite)	Colombia	U/Pb	1596 ± 52	Bonilla et al. (2019)
Marieta River, Marieta Granite	Venezuela	Rb/Sr	1340 ± 10	Cited in Barrios et al. (1985)
San Pedro Granite	Venezuela	Rb/Sr	1372 ± 10	Cited in Barrios et al. (1985)
Parguaza Granite	Venezuela	Rb/Sr	1386 ± 28	Cited in Barrios et al. (1985)
Parguaza Granite	Venezuela	Rb/Sr	1486 ± 25	Bogotá (1981)
Los Pijiguaos Granite	Venezuela	Rb/Sr	1531 ± 39	Gaudette et al. (1978)
Parguaza Granite	Venezuela	Rb/Sr	1531 ± 39	Bogotá (1981)
Marieta Granite	Venezuela	Rb/Sr	1534 ± 13	Barrios y Rivas (1980)
Parguaza Granite	Venezuela	U/Pb	1545 ± 20	Gaudette et al. (1978)
Intrusive suite Alto Candeias	Brazil	U/Pb	1338-1346	Bettencourt et al. (1999)
Intrusive suite Teotônio	Brazil	U/Pb	1387 ± 16	Bettencourt et al. (1999)
Intrusive suite Santo Antônio	Brazil	U/Pb	1406 ± 32	Bettencourt et al. (1999)
Mucajaí Granite	Brazil	U/Pb	1544 ± 42	Gaudette et al. (1996)
Içana River (two- mica grainite)	Brazil	Pb/Pb	1521 ± 32	Almeida et al. (1997)
Papuri River granite	Brazil	U/Pb	1521 ± 13	Tassinari et al. (1996)
Charnockite Serra da Prata	Brazil	U/Pb	1564 ± 21	Fraga et al. (1997)
Surucucú Granite	Brazil	Rb/Sr	1583	Dall'Agnol et al. (1975)
Intrusive suite Serra da Providencia	Brazil	U/Pb	1606 -1532	Bettencourt et al. (1999)

7.2.2 Age relations with Nb-Ta, U-Th bearing minerals

Melcher et al., (2017) based on U–Pb isotopes in wodginite–ixiolite, CGM, rutile and cassiterite, estimated a mineralization age ranging from 1453 to 1277 Ma for their Colombian samples, although they did not report their exact provenances.

For other hand samples of LOC (2) and Venezuela were mineralogically compared and rutile-(Nb,Ta) U-Pb ages are 1512 ± 12 Ma (Franco et al., 2021).

7.3 Intraplate tectono-magmatic phenomena and paleogeographic implications

Intraplate tectono-magmatic phenomena are generally attributed to the ascent of deep mantle plumes, arising from the core–mantle boundary. Mantle plumes are consistent with experimental studies and mantle seismic tomography. In addition, the assembly of supercontinents and their subsequent breakup are inferred to relate to the arrival of mantle plumes (Ernst, 2014). The rising of mantle plumes and/or asthenospheric melts results in tectonic and magmatic manifestations that include crustal uplifts, continental rifting, the emplacement of anorogenic magmas, and LIPs (large igneous provinces) on continents. Some of the most significant global anorogenic magmatic rocks of Earth's history are recognized in the period between 1300 and 1800 Ma (Ernst, 2014). For comparison, in Laurentia, a distinctive A-type or "anorogenic" granites of ~1.4 Ga age was emplaced heterogeneous Proterozoic crust see Goodge and Vervoort (2006), globally this magmatism according to conclusion in (Vigneresse, 2005) appears to be unique because it requires a supercontinent with a zone of juvenile crust surrounded by older cratons.

Huge Fe-Ti-V deposits hosted by anorogenic gabbro-anorthosite complexes, and A-type granite related systems enriched in elements such as Sn, W, Cu, Zn, Bi, Mo, U, and F are related to intraplate processes and mantle plume associated magmatism (Pirajno, 2007).

Based on the distribution of fragments of LIP of distinct ages, Chaves and Rezende (2019) have proposed a new reconstruction of Columbia (Nuna) supercontinent. This reconstruction is shown in Figure 10, where purple and green circles represent the thermal impact area promoted by 1.52 Ga and 1.38 Ga mantle plume activity, recorded by volcanic mafic dykes and sills (LIP fragments). The red circle in (Figure 10) corresponds to the studied area in the NW Amazon Craton, which probably suffered partial melting generating A-type granites and associated pegmatites with an age comparable to the one of mantle plumes.

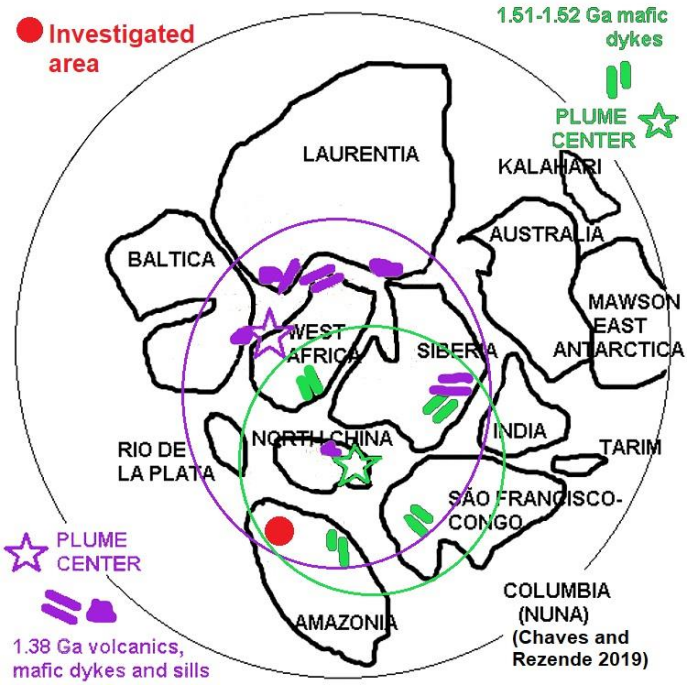

Figure 10. Columbia (Nuna) supercontinent reconstructed after Chaves and Rezende (2019). Purple and green circles represent the thermal impact area promoted by 1.52 Ga and 1.38 Ga mantle plume activity, recorded by their associated LIP fragments (volcanic, mafic dykes and sills). The red dot corresponds to the study area in the NW-Amazon Craton.

8 Conclusions

The monazite ages obtained by EPMA and LA-ICP-MS dating are in the same range for LOC (5) and (6) confirm that EPMA may be a useful tool to establish the crystallization age of monazite crystals poor in initial Pb. The high U, Th and radiogenic Pb contents and lack of inclusions and zonations of the homogeneous monazite crystals may make them suitable as internal standard material, however it would be necessary to find their primary source rocks, since there are age variations between the samples and the monazite grains from various primary sources may be in the same colluvial deposit.

The two age ranges suggest at least two enrichment events related with felsic intrusions and possibly associated pegmatites. The oldest ca. 1527 Ma processes forming CGM and the youngest of ca. 1346-1390 Ma forming REE and U-Th bearing minerals and in low proportion rutile-(Nb,Ta) and CGM.

The several kinds of ore minerals found in the three localities suggest different enrichment cycles linked to Mesoproterozoic magmatism. The Nb, Ta, U, Th and REE mineralizations may be result of pegmatitic phases of 1.52 Ga and 1.38 Ga anorogenic granitic magmatism triggered by mantle plumes affecting the Columbia (Nuna) supercontinent.

9 Acknowledgment

We wish to thank to the indigenous communities of Chorro Bocón, San Jose y Barranquilla for facilitating access to the study area, recognition, and sampling. This work would not have been possible without the support of the other members of GEGEMA group, mainly to PhD. Amed Bonilla Perez and Zeze Amaya Perea. We are indebted to the Universidad Nacional de Colombia which also gave financial support through the grant Hermes 35441 and to the Federal University of Minas Gerais. The Funds CTeI of the Sistema General de Regalías financed the project “Investigación de minerales estratégicos, industriales y materiales de construcción, Región Llanos” prompted by Colciencias and supervised by the Vaupés Department Government which allowed to realize field trips and large parts of the analysis. Two anonymous reviewers helped to improve the manuscript considerably.

10 References

Aarden, H., Davidson, M., 1977. Minerales de estaño, niobio, tántalo y titanio en la zona del Cano Aguamena, Estado Bolívar, analizados con microsonda de electrones, in: Memorias V Congreso Geológico Venezolano. Caracas, pp. 919–940.

Almeida, F.F.M. de, FIasui, Y., Brito-Neves, B.B. de, Fuck, R.., 1981. Brazilian structural provinces: an introduction. Earth Sci. Rev. 17, 1–29.

Amaral, G., 1974. Geologia pré-cambriana da região Amazônica.

Barrios, F., y Rivas, D., 1980. Reconocimientogeocronológico del Territorio Federal Amazonas, Venezuela. Bol. Soc. Venez. Geol. 21: 1-12.

Barrios, F., Cordani, H., y Kasawachita, K., 1985a.Caracterización Geocronológica del T.F. Amazonas,Venezuela. En VI Cong. Geol. Venezolano, 3: 1.432-1.480.

Barrios, F., Rivas, D., Cordani, U., and Kawashita, K.1985b. Geocronología del Territorio Federal Amazonas.In: Memoria I Simposium Amazónico, Puerto Ayacucho,Venezuela. Bol. Geol., Publ. Esp., 10: 22-31.

Bettencourt, J.S., Tosdal, R.M., Leite, W.B., Payolla, B.L., 1999. Mesoproterozoic rapakivi granites of the Rondo ˆ nia Tin Province , southwestern border of the Amazonian craton , Brazil — I . Reconnaissance U – Pb geochronology and regional implications 95, 41–67.

Bonilla-Pérez, A., Frantz, J.C., Charão-Marques, J., Cramer, T., Franco-Victoria, J.A., Mulocher, E., Amaya-Perea, Z., 2013. Petrography, geochemistry and geochronology of Parguaza granite in Colombia. Bol. Geol. 35.

Bonilla, A., Cramer, T., Poujol, M., Cano, H., Franco, J.A., Amaya, Z., 2019. Petrografía, geoquímica y geocronología U/Pb en circones de rocas ígneas y metamórficas a lo largo del Río Cuiarí en el sur del Departamento de Guainía, Colombia. Boletín Geol. 41, 55–84. https://doi.org/10.18273/revbol.v41n1-2019003

Bonilla, A., Frantz, J.C., Charão-Marques, J., Cramer, T., Franco, J.A., Amaya,

Z., 2016. Rapakivi magmatism in the middle Inirida Basin, Guainía deparment, Colombia. Bol. Geol. 38. https://doi.org/10.18273/revbol.v38n1-2016001

Bonilla, Amed (2019). Origen y evolución de los granitoides proterozoicos del Oriente Colombiano, noroeste del cratón amazónico.Universidad Nacional de Colombia, Doctoral thesis, Bogotá

Bonilla Perez, A., Franco, J.A., Cramer, T., Poujol, M., Cogné, N., Nachtergaele, S., De Grave, J., 2020. Apatite LA-ICP-MS U–Pb and fission-track geochronology of the Caño Viejita gabbro in E-Colombia: Evidence for Grenvillian intraplate rifting and Jurassic exhumation in the NW Amazonian Craton. J. South Am. Earth Sci. 98, 102438. https://doi.org/10.1016/j.jsames.2019.102438

Bonin, B., 2007. A-type granites and related rocks : Evolution of a concept , problems and prospects 97, 1–29. https://doi.org/10.1016/j.lithos.2006.12.007

Celada, C., Garzón, M., Gómez, E., Khurama, S., López, J., Mora, M., Navas, O., Pérez, R., Vargas, O., Westerhof, P., 2006. Potencial de Recursos Minerales en el Oriente Colombiano: Compilación y Análisis de la Información Geológica Disponible. INGEOMINAS, Bogotá - Colombia.

Černý, P., 1991. Rare-element granitic pegmatites. Part 1: Anatomy and internal evolution of pegmatite deposits. Geosci. Canada 18, 49–67.

Černý, P., Blevin, P.L., Cuney, M., London, D., 2005. Granite-related ore deposits. Econ. Geol. 100th Anniv. Vol. 337–370.

Černý, P., Ercit, T.S., 2005. The classification of granitic pegmatites revisited. Can. Mineral. 43, 2005–2026. https://doi.org/10.2113/gscanmin.43.6.2005

Cerný, P., London, D., Novák, M., 2012. Granitic Pegmatites as Reflections of Their Sources. Elements 8, 289–294. https://doi.org/10.2113/gselements.8.4.289

Chappell, B.W., White, A.J.R., 2001. Two contrasting granite types: 25 years later. Aust. J. Earth Sci. 48, 489–499. https://doi.org/10.1046/j.1440-0952.2001.00882.x

Chappell, B.W., White, A.J.R., 1974. Two contrasting granite types. Pacific Geol. 8, 173–174.

Chaves, A. de O., Oliveira, E.K. de, Garcia, L.R.A., 2013. Desenvolvimento do método de datação química U-Th-Pb de monazita por microssonda eletrônica na UFMG. Geonomos 21, 13–18. https://doi.org/10.18285/geonomos.v21i2.268

Chaves, A. de O. and Rezende, C. R., 2019, Fragments of 1.79-1.75 Ga Large Igneous Provinces in reconstructing Columbia (Nuna): a Statherian supercontinentsuperplume coupling?. EPISODES, v. 42, p. 55-67.

Cordani, U.G., Sato, K., Sproessner, W., Santos Fernandes, F., 2016. U-Pb zircon ages of rocks from the Amazonas Territory of Colombia and their bearing on the tectonic history of the NW sector of the Amazonian Craton. Brazilian J. Geol. 46, 5–35. https://doi.org/10.1590/2317-4889201620150012

Dall'Agnol, R., Costi, H.T., Leite, A.A. da S., de Magalhães, M.S., Teixeira, N.P., 1999. Rapakivi granites from Brazil and adjacent areas. Precambrian Res. 95, 9–39. https://doi.org/10.1016/S0301-9268(98)00125-9

Deer, W.A., Howie, R.A., Zussman, J., 2013. An Introduction to the Rock-Forming Minerals. Mineralogical Society of Great Britain and Ireland. https://doi.org/10.1180/DHZ

Dill, H.G., 2015. Pegmatites and aplites: Their genetic and applied ore geology. Ore Geol. Rev. 69, 417–561. https://doi.org/10.1016/j.oregeorev.2015.02.022

Dill, H.G., Melcher, F., Füßl, M., Weber, B., 2006. Accessory minerals in cassiterite: A tool for provenance and environmental analyses of colluvial–fluvial placer deposits (NE Bavaria, Germany). Sediment. Geol. 191, 171–189. https://doi.org/10.1016/j.sedgeo.2006.03.022

Eby, G.N., 1990. The A-type granitoids: A review of their occurrence and chemical characteristics and speculations on their petrogenesis. Lithos 26, 115–134. https://doi.org/10.1016/0024-4937(90)90043-Z

Engi, M., 2017, Petrochronology based on REE-Minerals: Monazite, Allanite, Xenotime, Apatite: Reviews in Mineralogy and Geochemistry, v. 83, p. 365 LP – 418.

Ernst, R.E., 2014. Large Igneous Provinces (1st edition). Cambridge University Press, Cambridge, p. 653.

Franco Victoria, J.A., 2015. Contribución a la geología histórica del Oriente Colombiano: Proveniencia de minerales metálicos con Nb, Ta, Mn, Fe, Ti, Sn y W, de un depósito laterizado, en cercanías a la Comunidad Indígena de Cachicamo, al NE del Departamento del Vichada. Universidad Nacional de Colombia, Tesis de Maestria, Bogotá, Bogotá.

Franco Victoria, J.A., Cramer, T., Bonilla-Pérez, A., Castañeda, A.J., Poujol, M., Amaya-Perea, Z., 2021. Mineralogía y geocronología de rutilo-(Nb,Ta) relacionado a casiterita y columbita-tantalita provenientes de rocas Mesoproterozoicas del Cratón Amazónico cerca de Cachicamo, Colombia. Bol. Geol. 43, 99–126. https://doi.org/10.18273/revbol

Frost, B.R., Frost, C.D., 2014. Essentials of igneous and metamorphic petrology. Cambridge University Press.

Galvis Vergara, J., Hugett, A., Ruge, P., 1979a. Proyecto Radargramétrico del Amazonas. La Amazonía Colombiana y sus recursos. Inst. Geográfico Agustín Codazzi, i 33–91.

Galvis Vergara, J., Huguett, A., Ruge, P., 1979b. Geología de la Amazonía Colombiana. Boletín Geológico, Boletín Geológico 22, 3–86.

Gandhi, S.M., Sarkar, B.C., 2016. Essentials of Mineral Exploration and Evaluation. Elsevier, Amsterdam, p. 408. https://doi.org/10.1016/B978-0-12-805329-4.00008-9

Gansser, A., 1974. The Roraima Problem (South America). Verhandl. Naturf. Ges., Basel 84, 80–100.

Gansser, A., 1954. The Guiana Shield (S. America) Geological Observations.

749 Eclog. Geol. Helvet 47, 77–112.

750 Gasquet D, Bertrand JM, Paquette J-L, Lehmann J, Ratzov G, De Ascencao
751 Guedes R, Tiepolo M, Boullier AM, Scaillet S, Nomade S, (2010) Miocene to
752 Messinian deformation and hydrothermalism in the Lauzière Massif (French
753 Western Alps): new U-Th-Pb and Argon ages. Bulletin de la Société
754 Géologique de France 181:227-241.

755 Gaudette, H.E., Mendoza, V.S., Hurley, P.M., Fairbairn, H.W., 1978. Geology and
756 age of the Parguaza rapakivi granite, Venezuela. Geol. Soc. Am. Bull. 89,
757 1335–1340. https://doi.org/10.1130/0016-
758 7606(1978)89<1335:GAAOTP>2.0.CO;2

759 Gaudette, H.E., Olszewski, W.J., 1985. Geochronology of the basement rocks,
760 Amazonas territory, Venezuela and Tectonic evolution of the western Guiana
761 Shield. Geol. en Mijnb. 64, 131–143.

762 Ginsburg, A.I., Timofeyev, I.N., Feldman, L.G., 1979. Principles of geology of the
763 granitic pegmatites. Nedra, Moscow.

764 Gómez Tapias, J., Nivia Guevara, Á., Montes Ramírez, N.E., Almanza Meléndez,
765 M.F., Alcárcel Gutiérrez, F.A., Madrid Montoya, C.A., 2015. Compilando la
766 geología de Colombia: Una visión a 2015. Imprenta Nacional de Colombia,
767 Bogotá.

768 Goodge, J.W., & Vervoort, J.D., 2006. Origin of Mesoproteroizoic A-type granites
769 in Laurentia: Hf isotope evidence. Earth and Planetary Science Letters, 243,
770 pp. 711- 731.

771 Henderson, P., 1984, Chapter 1 - General Geochemical Properties and
772 Abundances of the Rare Earth Elements, in Henderson, P. B. T.-D. in G. ed.,
773 Rare Earth Element Geochemistry: Elsevier, p. 1–32.

774 Herrera-Bangerter, G.C., 1989. Die proterozoischen Rapakivigranite von El
775 Parguaza (südliches Venezuela) - Dissertation. Universität Zürich.

776 Hiess, J., Condon, D.J., McLean, N., Noble, S.R., 2012. 238U/235U Systematics
777 in Terrestrial Uranium-Bearing Minerals. Science (80-.). 335, 1610–1614.
778 https://doi.org/10.1126/science.1215507

779 Huguett, A., Galvis, J., Ruge, P., 1979. La Amazonía Colombiana y sus recursos.
780 Geología, La Amazonía Colombiana y sus recursos. Proyecto
781 Radargramétrico del Amazonas. Bogotá.

782 Ibañez-Mejia, M., Ruiz, J., Valencia, V.A., Cardona, A., Gehrels, G.E., Mora, A.R.,
783 2011. The Putumayo Orogen of Amazonia and its implications for Rodinia
784 reconstructions: New U–Pb geochronological insights into the Proterozoic
785 tectonic evolution of northwestern South America. Precambrian Res. 191,
786 58–77. https://doi.org/10.1016/j.precamres.2011.09.005

787 Itano, K., Iizuka, T., Chang, Q., Kimura, J. I., and Maruyama, S., 2016, U–Pb
788 chronology and geochemistry of detrital monazites from major African rivers:
789 Constraints on the timing and nature of the Pan-African Orogeny:
790 Precambrian Research, v. 282, p. 139–156.

791 Itano, K., Iizuka, T., and Hoshino, M., 2018, REE-Th-U and Nd isotope
792 systematics of monazites in magnetite- and ilmenite-series granitic rocks of
793 the Japan arc: Implications for its use as a tracer of magma evolution and

detrital provenance: Chemical Geology, v. 484, p. 69–80.

Jercinovic, M.J., Williams, M.L., Lane, E.D., 2008. In-situ trace element analysis of monazite and other fine-grained accessory minerals by EPMA. Chem. Geol. 254, 197–215. https://doi.org/10.1016/j.chemgeo.2008.05.016

Kroonenberg, S.B., 2019. The Proterozoic Basement of the Western Guiana Shield and the Northern Andes, in: Cediel, F., Shaw, R.P. (Eds.), Geology and Tectonics of Northwestern South America. Springer International Publishing, Cham, pp. 115–192. https://doi.org/10.1007/978-3-319-76132-9_3

Kroonenberg, S.B., de Roever, E.W.F., Fraga, L.M., Reis, N.J., Faraco, T., Lafon, J.-M., Cordani, U., Wong, T.E., 2016. Paleoproterozoic evolution of the Guiana Shield in Suriname: A revised model. Netherlands J. Geosci. 95, 491–522. https://doi.org/10.1017/njg.2016.10

Larin, A. M., 2009, Rapakivi granites in the geological history of the earth. Part 1, magmatic associations with rapakivi granites: Age, geochemistry, and tectonic setting: Stratigraphy and Geological Correlation, v. 17, p. 235–258.

Laznicka, P., 2006. Giant Metallic Deposits - Future Sources of Industrial Metals. Springer.

London, D., 2018. Ore-forming processes within granitic pegmatites. Ore Geol. Rev. 101, 349–383. https://doi.org/10.1016/j.oregeorev.2018.04.020

London, D., Morgan, G.B., 2012. The Pegmatite Puzzle. Elements 8, 263–268. https://doi.org/10.2113/gselements.8.4.263

López Isaza, J.A., 2012. Unidades, petrografía y composición química del Complejo Migmatítico de Mitú en los alrededores de Mitú: Réplica. Boletín Geol. 34.

López Isaza, J.A., Cramer, T., 2012. Ambiente geológico del complejo Mitú y perspectivas de ocurrencias minerales de niobio y tantalio en el territorio colombiano. Geol. Colomb. 37, 75–95.

López Isaza, J.A., Khurama, S., Bernal Vargas, L.E., Cuéllar, M.A., 2007. El Complejo Mitú: una nueva perspectiva, in: Memorias Del XI Congreso Colombiano de Geología. Sociedad Colombiana de Geología, Bucaramanga, pp. 1–16.

López, J., Mora, B., Jiménez, D.M., Khurama, S., Marín, E., Obando, G., Páez, T.I., Carrillo, L.E., Bernal, L., 2010. Cartografía Geológica y Muestreo Geoquímico de las Planchas 297 – Puerto Inírida, 297 Bis – Merey Y 277 Bis – Amanaven, Departamento del Guainía. Ingeominas, Bogotá.

Ludwig, K.R., 2012. User´s manual for Isoplot 3.75 - A Geochronological Toolkit for Microsoft Excel, Berkeley Geochronology Center Special Publication No. 5.

Ludwig, K.R., 2003. User's Manual for Isoplot 3.00 - A Geochronological Toolkit for Microsoft Excel, Berkeley Geochronology Center Special Publication.

Magrini, D., Attanasio, D., Bracci, S., Cantisani, E., Prochaska, W., 2018. Innovative application of portable X-ray fluorescence (XRF) to identify Göktepe white marble artifacts. Archaeol. Anthropol. Sci. 10, 1141–1152.

https://doi.org/10.1007/s12520-016-0444-7

Mange, M.A., Wright, D.T. (Eds.), 2007. Heavy minerals in use, Developments in Sedimentology, 58, Developments in Sedimentology, 58.

Mariño-Pardo, N., 2012. Potencial minero del Bajo Parguaza. Rev. Commod. Venez. 2, 44–47.

Mariño, N., 2013. Coltán en Venezuela. Energía&Petróleo.

Melcher, F., Graupner, T., Gäbler, H.-E.E., Sitnikova, M., Oberthür, T., Gerdes, A., Badanina, E., Chudy, T., 2017. Mineralogical and chemical evolution of tantalum–(niobium–tin) mineralisation in pegmatites and granites. Part 2: Worldwide examples (excluding Africa) and an overview of global metallogenetic patterns. Ore Geol. Rev. 89, 946–987. https://doi.org/10.1016/j.oregeorev.2016.03.014

Montel, J.-M., Razafimahatratra, D., de Parseval, P., Poitrasson, F., Moine, B., Seydoux-Guillaume, A.-M., Pik, R., Arnaud, N., and Gibert, F., 2018, The giant monazite crystals from Manangotry (Madagascar): Chemical Geology, v. 484, p. 36–50.

Montel, J., Foret, S., Veschambre, M., Nicollet, C., and Provost, A., 1996, Chemical Electron microprobe dating of monazite: v. 1.

Mottana, A., Crespi, R., Liborio, G., Prinz, M., Harlow, G. E., and Peters, J., 1978, Simon and Schuster's guide to rocks and minerals: Simon and Schuster.

Paquette J-L, Tiepolo M, (2007) High resolution (5 μm) U-Th-Pb isotopes dating of monazite with excimer laser ablation (ELA)-ICPMS. Chemical Geology 240:222-237.

Perkins, D., 2014. Mineralogy, 3rd ed. Pearson Educación, Harlow.

Pinheiro, S.S., Fernández, P.E.C.A. Pereira, E.., Vasconcelos, E.., Pinto, A.., Montalvão, R.M.., Issler, R.., Dall'Agnol, R., Teixeira, W., Fernández, C.A.C., 1976. Geología - Projeto Radar na Amazônia. Folha NA.19-Pico da Neblina, in: Levantamento de Recursos Naturais- Vol 11. pp. 19–137.

Pirajno, F., 2007, Chapter 8.3 Ancient to Modern Earth: The Role of Mantle Plumes in the Making of Continental Crust, in Kranendonk, M. J. Van, Smithies, R. H., and Bennett, V. C. eds., Developments in Precambrian Geology:, p. 1037–1064.

Pirajno, F., 2009, Hydrothermal Processes and Mineral Systems: Dordrecht, Springer Netherlands, 1273 p.

Pommier, A., Cocherie, A., Legendre, O., 2004. EPMA Dating User'Manual, V. 1.01: Age Calculation from Electron Probe Microanalyser Measurements of U–Th–Pb. Brgm, Orleans.

Priem, H.N.A., Andriessen, P.A.M., Boelrijk, N.A.I.M., Boorder, H. de, Hebeda, E.H., Huguett, A., Verdurmen, E.A.T., Verschure, R.H., 1982. Geochronology of the Precambrian in the Amazonas Region of Southeastern Colombia (Western Guiana Shield). Geol. en Mijnb. 61, 229–242.

Poujol M, Pitra P, Van Den Driessche J, Tartèse R, Ruffet G, Paquette J-L, Poilvet J-C (2017) Two-stage partial melting during the Variscan extensional tectonics (Montagne Noire, France). Int J Earth Sci 106:477-500. doi:

10.1007/s00531-016-1369-1.

Reed, S.J.B., 2005. Electron Microprobe Analysis and Scanning Electron Microscopy in Geology, Electron Microprobe Analysis and Scanning Electron Microscopy in Geology. Cambridge University Press, Cambridge. https://doi.org/10.1017/CBO9780511610561

Santos, J.O.S., 2003. Geotectônica dos Escudos das Guianas e Brasil-Central. Geol. Tectônica e Recur. Minerais do Bras. 4, 169–195.

Santos, J.O.S., Hartmann, L.A., Gaudette, H.E., Groves, D.I., Mcnaughton, N.J., Fletcher, I.R., 2000. A new understanding of the Provinces of the Amazon Craton based on Integration of Field Mapping and U-Pb and Sm-Nd Geochronology. Gondwana Res. 3, 453–488. https://doi.org/10.1016/S1342-937X(05)70755-3

Santos, J.O.S., Potter, P.E., Reis, N.J., Hartmann, L.A., Fletcher, I.R., McNaughton, N.J., 2003. Age, source, and regional stratigraphy of the Roraima Supergroup and Roraima-like outliers in northern South America based on U-Pb geochronology. Geol. Soc. Am. Bull. 115, 331–348. https://doi.org/10.1130/0016-7606(2003)115<0331:ASARSO>2.0.CO;2

Santos, J.O.S., Rizzotto, G.J., Potter, P.E., McNaughton, N.J., Matos, R.S., Hartmann, L.A., Chemale, F., Quadros, M.E.S., 2008. Age and autochthonous evolution of the Sunsás Orogen in West Amazon Craton based on mapping and U-Pb geochronology. Precambrian Res. 165, 120–152. https://doi.org/10.1016/j.precamres.2008.06.009

SERVICIO GEOLÓGICO COLOMBIANO. 2013. Cartografía geológica y muestreo geoquímico de las planchas 201 BIS, 201, 200 Y 199 Departamento de Vichada. Memoria explicativa. Bogota

Scherrer, N.C., Eng, M., Gnos, E., Jakob, V., Liechti, A., 2000, Monazite analysis; from sample preparation to microprobe age dating and REE quantification. Schweizer Mineralogische und Petrographische Mitteilungen, v. 80, p. 93-105.

Sial, A.N., Bettencourt, J.S., Campos, C.P. De, Ferreira, V.P. (Eds.), 2011. Granite-related ore deposits, Geological Society, London, Special Publications. Geological Society, London, London. https://doi.org/10.1144/SP350.1

Sun, S.–., McDonough, W.F., 1989. Chemical and isotopic systematics of oceanic basalts: implications for mantle composition and processes. Geol. Soc. London, Spec. Publ. 42, 313–345. https://doi.org/10.1144/GSL.SP.1989.042.01.19

Suzuki, K., and Kato, T., 2008, CHIME dating of monazite, xenotime, zircon and polycrase: Protocol, pitfalls and chemical criterion of possibly discordant age data: Gondwana Research, v. 14, p. 569–586.

Tassinari, C.C.G., Macambira, M.J.B., 1999. Geochronological provinces of the Amazonian Craton. Episodes 22, 174–182. https://doi.org/10.1080/00206819709465329

Vermeesch, P., 2018. IsoplotR: A free and open toolbox for geochronology. Geosci. Front. 9, 1479–1493. https://doi.org/10.1016/j.gsf.2018.04.001

927 Vigneresse, J.L., 2005,The specific case of the Mid-Proterozoic rapakivi granites
928 and associated suite within the context of the Columbia supercontinent,
929 Precambrian Research, Volume 137, Issues 1–2, , Pages 1-34, ISSN 0301-
930 9268, https://doi.org/10.1016/j.precamres.2005.01.001.

931 Williams, M.L., Jercinovic, M.J., Hetherington, C.J., 2007, Microprobe Monazite
932 Geochronology : Understanding Geologic Processes by Integrating
933 Composition and Chronology.
934 https://doi.org/10.1146/annurev.earth.35.031306.140228

935 Williams, M. L., Jercinovic, M. J., Mahan, K. H., and Dumond, G., 2017, Electron
936 Microprobe Petrochronology: Reviews in Mineralogy and Geochemistry, v.
937 83, p. 153–182.

938 Winter, J. D., 1972, Introduction to Igneous and Metamorphic Petrology: Upper
939 Saddle River, New Jersey, Prentice Hall, 697 p.

940 Zhu, X. and O'Nions, R. 1999, Monazite chemical composition: some implications
941 for monazite geochronology. Contrib Mineral Petrol, 137, 351–363.
942 https://doi.org/10.1007/s004100050555

943

944

11 Annex, supplementary tables

Annex A. Supplementary table of operating conditions for the LA-ICP-MS equipment (GeOHeLiS Platform).

Laboratory & Sample Preparation

Laboratory name	GeOHeLiS Platform, University of Rennes, Rennes, France
Sample type/mineral	Monazite
Sample preparation	Separated grain mounted in epoxy pucks

Laser ablation system

Make, Model & type	ESI NWR193UC, Excimer
Ablation cell	ESI NWR TwoVol2
Laser wavelength	193 nm
Pulse width	< 5 ns
Fluence	5 J/cm^2
Repetition rate	3Hz
Spot size	8 µm
Sampling mode / pattern	Single spot
Carrier gas	100% He, Ar make-up gas and N2 (3 ml/mn) combined using in-house smoothing device
Background collection	20 seconds
Ablation duration	60 seconds
Wash-out delay	15 seconds
Cell carrier gas flow (He)	0.75 l/min

ICP-MS Instrument

Make, Model & type	Agilent 7700x, Q-ICP-MS
Sample introduction	Via conventional tubing
RF power	1350W
Sampler, skimmer cones	Ni
Extraction lenses	X type
Make-up gas flow (Ar)	0.85 l/min
Detection system	Single collector secondary electron multiplier
Data acquisition protocol	Time-resolved analysis
Scanning mode	Peak hopping, one point per peak
Detector mode	Pulse counting, dead time correction applied, and analog mode when signal intensity > ~ 10^6 cps
Masses measured	^{204}(Hg + Pb), ^{206}Pb, ^{207}Pb, ^{208}Pb, ^{232}Th, ^{238}U
Integration time per peak	10-30 ms
Sensitivity / Efficiency	22000 cps/ppm Pb (50µm, 10Hz)

Data Processing

Gas blank	20 seconds on-peak
Calibration strategy	Moacir monazite standard used as primary reference material, Managoutry monazite used as secondary reference material (quality control)

Reference Material info	Moacir (Gasquet et al., 2010) Manangoutry (Paquette and Tiepolo, 2007)
Data processing package used	GLITTER ® (van Achterbergh et al., 2001)
Mass discrimination	Standard-sample bracketing with $^{207}Pb/^{206}Pb$, $^{206}/^{238}U$, $^{208}Pb/^{232}Th$ normalized to reference material Moacir
Common Pb correction	No common Pb correction
Uncertainty level and propagation	Ages are quoted at 2 sigma absolute, propagation is by quadratic addition according to Horstwood et al. (2016). Reproducibility and age uncertainty of reference material are propagated.
Quality control / Validation	Manangoutry : 548 ± 6 Ma (MSWD=0.98 ; n=11)

Annex B. EPMA mineral chemistry data of monazite crystals from the localities Espina Hills LOC (4); San José LOC (5) and Barranquilla LOC (6) and ages calculated using Th, U and Pb contents. All elements are expressed as main oxides measure in weighted percent (wt.%) independently of their real oxidation state.

Sample	Analysis point/ oxide	P_2O_5	SiO_2	ThO_2	UO_2	Y_2O_3	La_2O_3	Ce_2O_3	Pr_2O_3	Nd_2O_3	Sm_2O_3	Gd_2O_3	Dy_2O_3	CaO	PbO	Total	U (ppm)	2σ %	Th (ppm)	2σ %	Pb (ppm)	2σ %	Age (Ma)	2σ (abs)
LOC4	1	27.99	1.05	8.65	0.27	1.38	10.83	30.00	3.04	10.75	2.90	1.18	0.64	1.49	0.57	100.73	1896	5.3	76016	1	5291	1.9	**1393**	45
	2	26.28	1.07	8.56	0.26	1.51	10.54	29.74	3.02	11.02	2.97	1.28	0.61	1.46	0.56	98.86	1813	5.5	75225	1	5198	1.9	**1387**	45
	3	26.32	1.16	8.14	0.18	1.45	11.00	30.23	3.04	11.27	2.77	1.23	0.60	1.13	0.51	99.02	1131	8.8	71534	1	4734	2.1	**1366**	48
	4	27.30	1.14	8.33	0.20	1.40	11.10	30.48	3.16	11.31	2.83	1.28	0.47	1.22	0.53	100.73	1297	7.7	73204	1	4920	2.0	**1378**	47
	5	26.08	1.37	8.51	0.18	1.41	11.00	30.23	3.25	11.52	2.60	1.19	0.51	0.94	0.55	99.32	1111	9.0	74786	1	5106	2.0	**1412**	47
	6	25.55	1.62	8.09	0.18	1.29	11.46	30.74	3.23	11.81	2.49	1.21	0.45	0.80	0.51	99.42	1134	8.8	71095	1	4734	2.1	**1374**	48
	7	26.15	1.04	8.65	0.28	1.48	10.71	29.31	2.96	10.86	2.89	1.21	0.68	1.45	0.58	98.23	1984	5.0	76016	1	5384	1.9	**1412**	45
LOC5	1	26.26	1.26	12.23	0.46	1.53	9.63	27.55	2.86	9.16	3.26	1.49	0.58	2.02	0.89	99.18	3371	3.0	107477	1	8262	1.2	**1502**	36
	2	27.61	1.19	11.95	0.44	1.22	9.95	28.21	2.95	9.49	3.40	1.52	0.50	1.91	0.87	101.21	3210	3.1	105017	1	8076	1.2	**1506**	37
	3	25.88	1.15	10.49	0.40	1.29	10.10	28.86	3.01	9.56	3.53	1.53	0.53	1.65	0.79	98.75	2939	3.4	92186	1	7334	1.4	**1549**	40
	4	26.40	1.06	9.56	0.35	0.98	10.49	30.38	3.08	9.93	3.48	1.46	0.32	1.52	0.69	99.69	2551	3.9	84013	1	6405	1.6	**1495**	42
	5	25.10	1.23	11.04	0.44	1.14	10.42	29.41	2.87	9.38	3.09	1.40	0.50	1.78	0.84	98.64	3261	3.1	97020	1	7798	1.3	**1556**	39
	6	25.39	1.20	11.14	0.44	1.20	9.83	27.86	2.88	9.66	3.34	1.36	0.49	1.85	0.83	97.47	3255	3.1	97898	1	7705	1.3	**1527**	38
	7	27.96	0.77	4.10	0.21	1.44	13.58	33.57	3.15	10.08	1.79	0.77	0.39	0.59	0.32	98.71	1578	6.3	36004	1.00	2933	3.41	**1529**	77
	8	27.49	1.34	5.86	0.27	1.55	12.35	32.03	3.31	10.95	2.22	1.10	0.37	0.72	0.45	100.00	2026	4.9	51506	1.00	4140	2.42	**1530**	59
LOC6	1	23.43	2.27	10.89	0.37	2.11	8.36	27.95	3.43	12.98	3.34	1.39	0.43	0.73	0.79	98.46	2652	3.8	95701	1	7334	1.4	**1514**	39
	2	24.17	2.20	10.72	0.34	2.15	8.39	27.91	3.41	12.85	3.40	1.28	0.44	0.73	0.78	98.77	2397	4.2	94207	1	7241	1.4	**1529**	40
	3	24.88	2.44	11.49	0.38	2.18	8.46	27.97	3.47	12.72	3.51	1.31	0.37	0.72	0.85	100.73	2707	3.7	100974	1	7891	1.3	**1547**	38
	4	24.27	2.08	10.07	0.35	1.94	8.60	28.78	3.22	13.15	3.57	1.33	0.32	0.69	0.74	99.10	2522	4.0	88495	1	6869	1.5	**1529**	41
	5	24.89	2.05	9.95	0.34	2.02	8.54	28.28	3.48	13.13	3.56	1.36	0.47	0.71	0.73	99.51	2441	4.1	87441	1	6777	1.5	**1530**	42
	6	25.27	2.12	10.12	0.34	2.12	8.65	28.19	3.38	13.02	3.66	1.31	0.52	0.68	0.74	100.11	2431	4.1	88935	1	6869	1.5	**1527**	41
	7	25.30	1.50	9.81	0.35	2.19	8.51	28.21	3.37	12.54	3.69	1.59	0.41	1.10	0.71	99.29	2537	3.9	86210	1	6591	1.5	**1503**	42

Sample	Analysis point/ oxide	P_2O_5	SiO_2	ThO_2	UO_2	Y_2O_3	La_2O_3	Ce_2O_3	Pr_2O_3	Nd_2O_3	Sm_2O_3	Gd_2O_3	Dy_2O_3	CaO	PbO	Total	U (ppm)	2σ %	Th (ppm)	2σ %	Pb (ppm)	2σ %	Age (Ma)	2σ (abs)
	8	24.89	1.87	11.07	0.39	2.06	8.56	26.92	3.22	12.71	3.55	1.50	0.52	1.17	0.81	99.24	2819	3.5	97283	1	7519	1.3	**1521**	39
	9	24.74	1.53	9.62	0.31	1.90	8.59	27.62	3.26	13.33	4.00	1.68	0.43	1.08	0.71	98.80	2195	4.6	84541	1	6591	1.5	**1548**	43
	10	25.66	1.76	10.61	0.34	2.08	8.55	27.08	3.39	12.77	3.82	1.46	0.39	1.27	0.77	99.95	2404	4.2	93241	1	7148	1.4	**1524**	40

1

2 Annex C. LA-ICP-MS U/Th/Pb isotopic data of monazite crystals from Espina Hills LOC (4), San José LOC (5) and Barranquilla LOC (6).

Points of ablation	$^{208}Pb/^{232}Th$	PropErr2σAbs	$^{206}Pb/^{238}U$	PropErr2σAbs	$Age^{206}Pb/^{238}U$	PropErr2σAbs	$Age^{208}Pb/^{232}Th$	PropErr2σAbs
Mnz_Loc (4) p1	0.0670	0.0051	0.230	0.016	1327	22	1311	14
Mnz_Loc (4) p2	0.0660	0.0050	0.230	0.016	1327	26	1291	16
Mnz_Loc (4) p3	0.0716	0.0054	0.238	0.017	1377	22	1397	17
Mnz_Loc (4) p4	0.0685	0.0052	0.239	0.017	1380	19	1339	15
Mnz_Loc (4) p5	0.0673	0.0051	0.229	0.016	1322	22	1316	16
Mnz_Loc (4) p6	0.0697	0.0052	0.233	0.016	1352	29	1361	17
Mnz_Loc (4) p7	0.0690	0.0053	0.238	0.016	1371	22	1350	16
Mnz_Loc (4) p8	0.0687	0.0053	0.239	0.017	1379	22	1343	16
Mnz_Loc (4) p9	0.0636	0.0051	0.230	0.016	1325	55	1245	26
Mnz_Loc (4) p10	0.0676	0.0052	0.233	0.016	1347	30	1321	19
Mnz_Loc (4) p11	0.0637	0.0049	0.231	0.016	1334	28	1248	15
Mnz_Loc (4) p12	0.0683	0.0052	0.233	0.016	1345	27	1334	20
Mnz_Loc (4) p13	0.0664	0.0051	0.232	0.016	1340	23	1298	16
Mnz_Loc (4) p14	0.0696	0.0053	0.238	0.016	1374	22	1360	16
Mnz_Loc (4) p15	0.0686	0.0053	0.238	0.016	1373	23	1341	18
Mnz_Loc (4) p16	0.0683	0.0052	0.240	0.017	1383	22	1335	16
Mnz_Loc (4) p17	0.0711	0.0054	0.244	0.017	1406	21	1388	16
Mnz_Loc (4) p18	0.0662	0.0051	0.231	0.016	1331	26	1294	17
Mnz_Loc (4) p19	0.0672	0.0051	0.236	0.017	1356	30	1314	16

Mnz_Loc (4) p20	0.0673	0.0051	0.236	0.016	1360	20	1315	15
Mnz_Loc (4) p21	0.0703	0.0054	0.243	0.017	1399	20	1371	16
Mnz_Loc (4) p22	0.0679	0.0052	0.235	0.016	1361	19	1326	13
Mnz_Loc (5) p1	0.0801	0.0036	0.265	0.011	1511	55	1556	67
Mnz_Loc (5) p2	0.0796	0.0036	0.265	0.010	1513	53	1547	67
Mnz_Loc (5) p3	0.0824	0.0037	0.276	0.011	1569	57	1599	70
Mnz_Loc (5) p4	0.0801	0.0037	0.268	0.011	1523	56	1556	69
Mnz_Loc (5) p5	0.0761	0.0034	0.258	0.010	1474	53	1482	64
Mnz_Loc (5) p6	0.0787	0.0035	0.264	0.010	1505	53	1530	66
Mnz_Loc (5) p7	0.0753	0.0034	0.256	0.011	1465	54	1468	63
Mnz_Loc (5) p8	0.0764	0.0034	0.255	0.010	1461	52	1488	64
Mnz_Loc (5) p9	0.0783	0.0035	0.259	0.010	1482	53	1523	65
Mnz_Loc (5) p10	0.0767	0.0034	0.259	0.010	1481	51	1492	64
Mnz_Loc (5) p11	0.0828	0.0037	0.273	0.011	1553	58	1606	69
Mnz_Loc (5) p12	0.0808	0.0036	0.270	0.011	1540	55	1570	67
Mnz_Loc (5) p13	0.0827	0.0037	0.275	0.011	1560	58	1606	69
Mnz_Loc (5) p14	0.0809	0.0036	0.273	0.011	1549	55	1571	67
Mnz_Loc (6) p1	0.0784	0.0035	0.262	0.011	1499	56	1525	66
Mnz_Loc (6) p2	0.0780	0.0035	0.260	0.010	1488	53	1517	65
Mnz_Loc (6) p3	0.0771	0.0034	0.259	0.011	1481	55	1500	64
Mnz_Loc (6) p4	0.0851	0.0038	0.281	0.011	1596	57	1649	70
Mnz_Loc (6) p5	0.0817	0.0036	0.273	0.011	1554	55	1587	68
Mnz_Loc (6) p6	0.0793	0.0035	0.267	0.010	1522	53	1543	66
Mnz_Loc (6) p7	0.0770	0.0034	0.259	0.010	1482	53	1499	64
Mnz_Loc (6) p8	0.0861	0.0039	0.305	0.012	1710	60	1669	72
Mnz_Loc (6) p9	0.0783	0.0035	0.258	0.011	1477	56	1522	66
Mnz_Loc (6) p10	0.0801	0.0036	0.270	0.011	1534	54	1557	67
Mnz_Loc (6) p11	0.0827	0.0037	0.272	0.011	1545	55	1605	69
Mnz_Loc (6) p12	0.0791	0.0036	0.267	0.011	1520	55	1538	67
Mnz_Loc (6) p13	0.0803	0.0036	0.263	0.010	1500	52	1560	67
Mnz_Loc (6) p14	0.0785	0.0035	0.260	0.010	1485	52	1527	65